SECURITY INFORMATION

Copy 202

RM A53H18

NACA RM A53H18

TECH LIBRARY KAFB, NM
01435b2

6419

NACA

RESEARCH MEMORANDUM

A METHOD FOR ESTIMATING THE ROLLING MOMENTS CAUSED BY WING-TAIL INTERFERENCE FOR MISSILES AT SUPERSONIC SPEEDS

By Sherman Edwards and Katsumi Hikido

Ames Aeronautical Laboratory
Moffett Field, Calif.

CLASSIFIED DOCUMENT

This material contains information affecting the National Defense of the United States within the meaning of the espionage laws, Title 18, U.S.C., Secs. 793 and 794, the transmission or revelation of which in any manner to an unauthorized person is prohibited by law.

NATIONAL ADVISORY COMMITTEE
FOR AERONAUTICS

WASHINGTON

November 12, 1953

CONFIDENTIAL

Classification canc'd (or changed to UNCLASSIFIED)

By Authority of NASA Tech Pub Announcement #1
(OFFICER AUTHORIZED TO CHANGE)

By 14638
NAME AND

GRADE OF OFFICER MAKING CHANGE)

28 Mar 61
DATE

TECH LIBRARY KAFB, NM
0143362

1P

NATIONAL ADVISORY COMMITTEE FOR AERONAUTICS

RESEARCH MEMORANDUM

A METHOD FOR ESTIMATING THE ROLLING MOMENTS CAUSED BY WING-TAIL INTERFERENCE FOR MISSILES AT SUPERSONIC SPEEDS

By Sherman Edwards and Katsumi Hikido

SUMMARY

A method is presented for estimating the rolling moments caused by wing-tail interference for missiles composed of wing-tail-body combinations. The considerations involved in estimating the structure of the downwash field behind lifting cruciform wing-body combinations and in estimating the induced rolling moments on cruciform tail surfaces trailing in this downwash field are discussed in detail. Estimates of the induced rolling moments for several missile configurations are shown to compare reasonably with the experimental results.

INTRODUCTION

Interference phenomena can exert a strong influence on the aerodynamic characteristics of missiles; consequently, the accuracy of estimates of stability and control parameters is a direct function of the precision with which these interference phenomena can be computed. Missile interference problems, in general, can be divided into three categories: wing-wing, wing-body, and wing-tail interference. The wing-wing and wing-body types of interference have been the subject of a number of theoretical and experimental investigations (refs. 1 through 10) and are relatively well understood. In contrast, an understanding of the mechanism of wing-tail interference, until very recently, has been lacking, and, as a result, the search for missile configurations having desirable stability and control characteristics has been handicapped.

An attempt was made in reference 10 to compute wing-tail interference effects and the resulting longitudinal stability characteristics of an air-to-air missile having a cruciform wing and tail. This

[redacted]

analysis indicated that the pitching moments of missiles having lifting surfaces arranged in tandem were amenable to calculation. The results encouraged the extension of these methods to the study of tail rolling moments resulting from wing-tail interference. At least three conditions can be enumerated in which such rolling moments occur for missiles composed of tandem arrangements of cruciform wings:

1. When all surfaces of the wing are fixed at zero incidence and the airframe is at combined angles of attack and bank.

2. When the forward wing surfaces are differentially deflected.

3. When a variable-incidence-wing missile is at an angle of attack (at zero bank angle) and the missile receives a signal which results in large deflections of the forward vertical wing panels.

The extension of the methods of reference 10 has been aimed at estimating the effect of the third condition; however, the method should apply equally well to the other cases. It is the purpose of this report to present the method and to apply it to several missile configurations for which experimental results are available.

NOTATION

a	body radius, ft
c_r	root chord, ft
C_{l_t}	rolling-moment coefficient on the trailing wing (tail) of a tandem wing missile (positive for clockwise as viewed upstream), $\frac{\text{rolling moment}}{qS_t 2s_t}$
C_N	normal-force coefficient (based upon the exposed area of one wing panel), $\frac{\text{normal force on one wing panel}}{qS_w}$
C_{L_α}	lift-curve slope, $\frac{\partial C_L}{\partial \alpha}$, per radian
d	body diameter, ft
e	distance from body center line to an image vortex inside the body, ft
f	distance from body center line to a vortex external to the body, ft

h_{CF} magnitude of the deflection of a streamline caused by the induced crossflow about the body, ft

h magnitude of the deflection of a streamline induced by an infinite line vortex, ft

k crossflow velocity ratio, $\frac{q_{CF}}{V_o \sin \alpha}$

K number of incremental distances in the graphical construction

l_t distance from the trailing edge of a wing to a point in the stream behind the wing at which the structure of the downwash field is desired, ft

L_t' rolling moment (positive for clockwise moments as viewed upstream), lb ft

$\left(\frac{l}{q_o \epsilon}\right)$ strip loading per unit angle of attack, ϵ, in terms of the dynamic pressure

M_o Mach number

q velocity at any point induced by an infinite line vortex, $\frac{\Gamma}{2\pi r}$, ft/sec

q_{CF} magnitude of the induced velocity caused by the crossflow about the body, $kV_o \sin \alpha$, ft/sec

q_o dynamic pressure, $\frac{1}{2} \rho_o V_o^2$, lb/sq ft

r radial distance from the center of a vortex, ft

R roll-influence function

s' distance from the body center line to the center of gravity of the vortex sheet discharged from a wing panel, ft

s_t semispan of the trailing wing of a tandem wing missile, ft

S_t gross area in one plane of the trailing wing (including the area within the body obtained by extending trailing and leading edges of the wing to the body center line), sq ft

S_w exposed area of one forward wing panel, sq ft

[redacted]

t	time, sec
V_o	free-stream velocity, ft/sec
(v,w)	sidewash and upwash velocities (positive in the positive directions of y' and z' axes, respectively, see fig. 1), ft/sec
X	complex coordinate $(y + iz)$, dimensionless
(x',y',z')	Cartesian coordinate system with positive direction of x' downstream along the body center line, the x', z' plane vertical, and y' measured positively to the right looking upstream (body axes), ft
(x,y,z)	Cartesian coordinate system in terms of s_t
(y_1,z_1)	coordinates of an infinite line vortex with respect to a cruciform wing in terms of the semispan, s_t
α	angle of attack, radians unless specified
β	$\sqrt{M_o^2 - 1}$
Γ	Circulation (positive for clockwise circulation of trailing vortex as viewed upstream), ft^2/sec
ϵ_v	sidewash angle, $\frac{v}{V_o}$, radians
ϵ_h	downwash angle, $-\frac{w}{V_o}$, radians
ρ_o	stream mass density, slugs/cu ft
σ	complex coordinate in the transformed plane $(\tau + i\nu)$
Φ	complex potential in the σ plane
φ	velocity potential in the σ plane
φ'	velocity potential in the X plane

METHOD OF ANALYSIS

In the course of the investigation, it was found that the analysis could be divided into two main phases: first, the problem of estimating

the induced flow field behind a lifting cruciform wing-body combination and, second, the problem of calculating the rolling moment induced on a cruciform wing in this nonuniform flow.

INDUCED FLOW BEHIND LOW-ASPECT-RATIO CRUCIFORM WING-BODY COMBINATIONS

Treatment of wing-tail interference effects depends in a large measure on an understanding of the manner in which vorticity is discharged from cruciform wings in combination with a body and upon an adequate representation of the resulting induced flow downstream. The complex nature of the real vortex sheets, however, precludes an exact representation in any practical computation procedure and indicates that a simplified model should be chosen.

The model selected for the present study is illustrated in figure 1, which shows a typical cruciform wing-body combination with the simplified model of the vortex system. This model is similar to that used in reference 10 to compute the effects of wing-tail interference upon missile pitching moments. In this model the vorticity discharged from each panel of the combination is considered to be completely rolled up into a discrete vortex immediately behind the trailing edge of each panel. In accordance with this assumption, each wing panel in figure 1 is replaced by a bound vortex and two trailing line vortices, one near the tip of the wing at the center of gravity of the vortex sheet discharged from the panel, the other within the body at a point corresponding to the image position of the external vortex.

In order to use this vortex model to calculate the induced flow downstream of the wing, one must estimate:

1. The strength and origin of the vorticity at the wing trailing edge.

2. The paths of the vortices as they trail downstream.

The procedures and assumptions involved in each of these steps are summarized in the following sections.

Vortex Strength and Origin

At present, the discharge of vorticity from cruciform wing-body combinations at supersonic speeds is not clearly understood, particularly with regard to the effects of large angles of attack and angles

of sideslip. It is not the purpose of this discussion to dwell upon this problem but to present a simplified vortex model which, although it disregards some recognized phenomena (see ref. 11), appears to provide a reasonable basis for computations.

For certain wing plan forms, the span loading of the wing is insensitive to sideslip, and a simple, direct relationship between span loading and circulation can be used. The application of this simple relationship to low-aspect-ratio triangular wings for which the span loading varies with angle of sideslip, however, is the subject of controversy. A study of linear theory indicates its use to be incorrect since linear theory, while predicting an asymmetry of loading, indicates that, for small angles of sideslip, the spanwise distribution of circulation remains symmetric. The relation between circulation distribution and span loading, valid at zero sideslip, therefore, does not hold for wings in sideslip. A study of the experimental evidence, references 10 and 12, on the other hand, and of rough theoretical approximations for large angles of sideslip indicates that a simple, direct relation between load and circulation gives a reasonable approximation of the correct vortex strength for cruciform wing-body combinations at supersonic speed. In the present instance, the simple relationship applied to all wings to determine the strength of the vortex filaments is as follows:[1]

$$\Gamma_n = \frac{C_{N_n} V_o S_w}{2[s' - (a^2/s')]} \qquad (1)$$

The denominator of this equation is determined from the position of the vortex center of gravity which is estimated by replacing the spanwise load distribution on a panel by an equivalent rectangular loading. This estimation is based on the meager data available (refs. 11 through 14).

The reader should note that in the analysis, body crossflow vortices (refs. 15 and 16) are not treated.

[1]This equation assumes that the panels of a cruciform wing are aerodynamically independent (wing-wing interference disregarded). This independency was found to have a significant effect upon induced-roll computations applied to missiles for which the loading on the forward wing is influenced appreciably by sideslip angle. This point is discussed further on page 23.

Vortex Paths Downstream of Simplified Model

Unfortunately, simple equations which define uniquely the paths of the vortices downstream of the simplified model previously discussed cannot be written (ref. 17). The methods which are available for determining the vortex motions are rather tedious inasmuch as they involve numerical procedures for computing the effects of mutual interference between the vortices and the effect of the flow about the body. As a step toward reducing the labor required in evaluating these effects, a graphical computing procedure is presented.

With the assumption that the bound vortices within the wing are unimportant in determining the structure of the induced flow field downstream (ref. 18), the simplified model (fig. 1) consists of eight infinite line vortices. Four of the vortices are situated outside an infinite circular cylinder representing the body and are free to move along the streamlines downstream of the wing trailing edge; the other four vortices are inside the cylinder at the image points determined from the positions of the external vortices. At each station along the missile body, the rotational axes of all vortices are considered to be parallel to the body center line. The complicated three-dimensional flow about a cruciform wing-body combination reduces, then, to a two-dimensional flow in planes normal to the center line of the body. The paths of the streamlines downstream of the wing, therefore, can be approximated by examining the flow in successive crossflow planes and by determining the deflections of the streamlines between each of these planes. To accomplish this objective, the tail length (l_t) is divided into an arbitrary number of equal increments, say K increments. The time required for the stream to traverse one increment is, then

$$t = \frac{l_t}{KV_o} \tag{2}$$

In this time interval, deflections of the streamlines and corresponding changes in the spatial relationship between the rotational axes of the eight vortices of the simplified model, both with respect to the body and with respect to each other, occur because of:

1. The presence of the body.

2. The mutual interaction between the four external and four image vortices representing the simplified model of the lifting wing-body combination.

Expressions for obtaining each of these deflections are presented in the following paragraphs.

If it is assumed that the crossflow about the body can be represented by a two-dimensional flow about an infinite circular cylinder, then the deflection in the time interval t (of the streamline which intersects a particular crossflow plane at any given point) caused by the body is

$$\frac{h_{CF}}{d} = \frac{q_{CF}}{d}\frac{l_t}{KV_o} = k\left[\left(\frac{l_t}{Kd}\right)\sin\alpha\right] \tag{3}$$

where k is given by

$$k = \sqrt{1 - \frac{2(z^2 - y^2) - 1}{(z^2 + y^2)^2}}$$

The constant k is simply the ratio of the fluid velocity at any point in the two-dimensional flow about a circular cylinder to the undisturbed velocity at infinity ($V_o \sin\alpha$). Values of k are between 0 and 2.

The presence of an infinite line vortex with its axis of rotation normal to this crossflow plane causes the streamline being considered to be deflected a distance given by

$$\frac{h_{\Gamma_n}}{d} = \frac{q}{d}\frac{l_t}{KV_o} = B\left(\frac{d}{r}\right) \tag{4}$$

where

$$B = \frac{C_{N_n}}{4\pi K}\left(\frac{S_w}{d^2}\right)\left(\frac{l_t}{d}\right)\left(\frac{d}{s' - a^2/s'}\right)$$

The terms in the parameter B are obtained by substituting for the vortex strength Γ and time interval t from equations (1) and (2), respectively. As a further consideration regarding the induced effects of vortices in the flow field, the relationship between a vortex and its image inside a cylinder is a constraint which somewhat simplifies the graphical procedure. This condition is expressed by

$$\frac{e}{d}\frac{f}{d} = \frac{1}{4} \tag{5}$$

Equations (3) through (5) form the basis for the graphical constructions and are incorporated into the charts shown in figure 2. In order to improve the accuracy of the graphical computations, tabulated values of the parameters necessary to draw these charts to a larger scale are given in tables I and II. These charts are designed to be used as underlays in the graphical procedure, the details of which are discussed in Appendix A.

ROLLING MOMENT ON CRUCIFORM WINGS INDUCED BY AN INFINITE LINE VORTEX

In the previous section, a graphical procedure was presented for tracing the paths of vortices shed from the forward lifting surfaces of a tandem-wing missile downstream to the vicinity of the trailing wing. The induced flow in this region is assumed, then, to be that caused by a number of discrete vortices with a specified spatial orientation and strength. The problem of computing the rolling moment on a wing immersed in this flow field can be resolved by solving first the general problem involving one vortex with its rotational axis parallel to the root chord of the wing. The rolling moment caused by more than one vortex, then, is determined by adding the contribution of each individual vortex. Theoretical considerations involved in the solution of this phase of the problem are divided in the following sections, according to the relationship between the sweep of the Mach lines and the sweep of the wings as follows:

1. Wings with supersonic leading edges.

2. Triangular wings with subsonic leading edges.

3. Slender triangular wings lying near the center of the Mach cone.

Wings With Supersonic Leading Edges

Pertinent geometric relationships involved in solving for the rolling moment induced by an infinite line vortex on cruciform wings in this category are shown in figure 3. The rolling-moment coefficient will be expressed in terms of the area, S_t, and the maximum span, $2s_t$, of the wing in one plane of the cruciform and will be related to the nondimensional aerodynamic and geometric parameters obtained previously in the development of the simplified model. Viewed from the rear, clockwise rotation of the flow due to a vortex and clockwise rolling moments are considered positive.

Determination of the local induced flow angle perpendicular to the planar components of the cruciform wing.- With reference to the geometric relationships given in figure 3, the velocity at any point in the flow field about the vortex is,

$$q = \frac{\Gamma}{2\pi r}$$

from which it may be determined that the local induced-flow angles in the horizontal and vertical planes are,

$$\epsilon_h = -\frac{w}{V_o} = \frac{\Gamma}{2\pi V_o s_t} \frac{(y-y_1)}{(y-y_1)^2 + z_1^2} \tag{6}$$

and

$$\epsilon_v = \frac{v}{V_o} = \frac{\Gamma}{2\pi V_o s_t} \frac{(z-z_1)}{(z_1-z)^2 + y_1^2} \tag{7}$$

Rolling moment on the wing.- A number of methods are available for determining the loads on lifting surfaces in nonuniform flow fields (see Appendix of ref. 10). The approach based upon reversed-flow relations is particularly useful from the standpoint of general applicability and, in many cases, reduced complexity of the computations. A discussion of these reciprocity relations as applied to aerodynamic problems including a list of references on the subject is contained in reference 19. Reversed-flow theorems are utilized in the present analysis wherever their application results in simplification of the computations.

In order to find the rolling moment on a cruciform wing situated in the nonuniform flow given by equations (6) and (7), it is necessary to determine the appropriate roll-influence function for the wing, which is equivalent to finding the span loading on the wing rolling at the rate of one radian per second in reversed flow (ref. 20). The roll-influence function depends directly upon the wing plan form and Mach number. In this section, the roll-influence functions for rectangular wings (of high aspect ratio) and triangular wings of cruciform arrangement will be determined; a family of wings whose roll-influence functions fall between those of high-aspect-ratio rectangular wings and triangular wings also will be discussed. It is believed that by suitable interpolation between the results for these cases, estimations of the rolling moment induced by an infinite line vortex on a large class of wings with supersonic leading edges can be made.

If tip effects for the rectangular wing are disregarded, the roll-influence function (or the spanwise loading on the rolling wing) obtained either by means of strip theory or by the use of the reversed-flow theorem, is a linear function of the span variable and is given by

$$R(y) = \left(\frac{l}{q_o \epsilon}\right) y = \frac{4}{\beta} \frac{c_r}{s_t} y \tag{8}$$

From a consideration of reverse-flow principles, it can be shown that the roll-influence function for triangular wings (horizontal components) with supersonic edges is a parabolic function of the span variable given by the equation

$$R(y) = \left(\frac{l}{q_o \epsilon}\right) y = \frac{4}{\beta} \frac{c_r}{s_t} (1 - |y|) y \tag{9}$$

These results may be combined in the form of the following more general equation:

$$R_m(y) = \left(\frac{l}{q_o \epsilon}\right) y = \frac{4}{\beta} \frac{c_r}{s_t} (1 - |y|^m) y \tag{10}$$

which is plotted in figure 4 for various values of m. Note that for values of y less than 1, equation (10) reduces to equation (8) as m becomes infinite. For this case, the function is discontinuous when y equals 1. When m equals 1, equation (10) is identical to equation (9). When the exponent m takes various values between 1 and ∞, roll-influence functions between those for the high-aspect-ratio rectangular wing and the triangular wing are obtained.

If it is assumed that the interference between the horizontal and vertical components of a cruciform wing with supersonic edges can be disregarded, the roll-influence function for the vertical wing component $R_m(z)$ (see fig. 3) is identical to that of the horizontal wing components with the substitution of z for the y variable. The interference between the two planar components of the cruciform wing is confined to the region within the Mach cone originating at the point of intersection of the leading edges of the wing components. As the area of the wing within this Mach cone decreases relative to the total wing area, the assumption that the two components of the cruciform wing do not interfere improves. Such a condition occurs with increasing aspect ratio and/or Mach number. The rolling moment on the wing, then, induced by the nonuniform downwash field described by equations (6) and (7) is, in coefficient form,

$$C_{l_t} = \frac{s_t^2}{2S_t} \left[\int_{-1}^{1} R_m(y) \epsilon_h \, dy + \int_{-1}^{1} R_m(z) \epsilon_v \, dz \right]$$

Upon substitution for the induced-flow-angle expressions and roll-influence function from equations (6), (7), and (10), this equation becomes

$$C_{l_t} = \frac{\Gamma s_t}{\pi \beta V_o S_t} \left(\frac{c_r}{s_t}\right) F_m \tag{11}$$

where

$$F_m = \int_{-1}^{1} \frac{(1 - |y|^m)(y - y_1) y \, dy}{(y - y_1)^2 + z_1^2} + \int_{-1}^{1} \frac{(1 - |z|^m)(z - z_1) z \, dz}{(z_1 - z)^2 + y_1^2}$$

The integrals in the parameter F_m have been computed for values of the exponent m of infinity (corresponding to the rectangular wing of high aspect ratio), four, two, and one (corresponding to the triangular wing with supersonic edges). The results are presented in figure 5. The curves on these charts are the loci of vortex positions with respect to the cruciform wing for which the rolling moment induced by a vortex of given strength is constant. These curves were obtained by cross-plotting the integral values of F_m for various positions of a line vortex given by the coordinates y_1, z_1. The charts are drawn only for vortex positions in the first quadrant of the coordinate system shown in figure 3. Since conditions of symmetry exist, however, the entire field may be completed by simple reflection. The sign of the parameter, F_m, is in accordance with the sign convention adopted previously; that is, induced flow about the vortex in a clockwise manner, when viewed from the rear, is considered positive. For counterclockwise vortex rotation, the sign of the parameter as determined from figure 5 is simply reversed. It is interesting to note the similarity between the charts for various values of the exponent m and also the existence, in each case, of vortex positions for which the rolling moment on the wing is zero regardless of the vortex strength ($F_m = 0$).

Rolling moment on the trailing cruciform wing in relation to the simplified model.- The expression for the rolling-moment coefficient given in equation (11) can be related to the simplified model described previously through the medium of the vortex strengths Γ which are preserved in the flow downstream from the forward wing. From equation (1), the vortex strength for the simplified model was

$$\Gamma_n = \frac{C_{N_n} V_o S_w}{2[s' - (a^2/s')]}$$

If the normal-force coefficient C_{N_n} in this expression is based now upon the gross area S_t of the trailing wing in one plane of the cruciform and the lifting-line length $s' - a^2/s'$ is measured in terms of the semispan of the trailing wing s_t, then

$$\Gamma = \frac{G V_o S_t}{2 s_t} \tag{12}$$

where,

$$G = \left(C_{N_n} \frac{S_w}{S_t}\right) \left[\frac{s_t}{s' - (a^2/s')}\right] \tag{13}$$

Upon substitution of Γ from equation (12) into equation (11), the rolling-moment coefficient becomes

$$C_{l_t} = \frac{G}{2\pi\beta} \frac{c_r}{s_t} F_m \tag{14}$$

where G is defined by equation (13) and F_m is determined from the charts in figure 5.

For rectangular wings of high aspect ratio and triangular wings with supersonic edges, of course, the values of F_m are taken from figures 5(a) and 5(d), respectively. An analysis of the rolling moment induced by a vortex on cruciform wings of other plan forms in this category would require a reconsideration of equation (14) for each change in the parameters which determine the roll-influence function, namely, plan form and Mach number. Obviously, such a procedure could become very involved. It is believed that by comparison of the computed roll-influence function for the wing being considered (or the span loading on the rolling wing in reversed flow) with the roll-influence functions plotted in figure 4, estimation of an approximate value of the exponent m from this comparison, then interpolation between the charts of figure 5, the induced rolling-moment characteristics of a large class of wings in this category can be estimated. For design purposes, it is probably sufficient to bracket the rolling moments by over and under approximations, and determine F_m from two of the charts presented in figure 5 without recourse to interpolation. In some cases, of course, the roll-influence function for a wing is not approximated with sufficient accuracy by any of the curves of figure 4 or by any combination of these influence functions. In order to compute the rolling moment for wings of this type, it will be necessary to construct a chart similar to those of figure 5, based upon the roll-influence function for the particular wing being considered; or, if values of the rolling moment are required for only a few critical maneuvering conditions of flight, these moments can be obtained by evaluating the appropriate integrals.

Triangular Wings With Subsonic Leading Edges

The rolling moments induced by an infinite line vortex on cruciform wings of triangular plan form with the leading edges of the wing swept behind the Mach cone will be considered in this section. With reference to the geometric relations shown in figure 3, the distributions of downwash and sidewash on the horizontal and vertical components of the wing are given again by equations (6) and (7), respectively. Again, in this case, it will be assumed that interaction between the horizontal and vertical components of the wing is negligible; therefore, each component can be treated as an independent planar wing system. This assumption is probably satisfactory provided the leading edges of the wing are not swept far behind the Mach cone, in which case interaction between the wing components assumes a more predominant role. This case will be treated in the following section.

The spanwise distribution of the lift on a planar triangular wing with subsonic edges is known to be elliptical and can be expressed as

$$\frac{l}{q_o \epsilon} = \frac{2 S_t C_{L_{\alpha_t}}}{s_t^2 \pi} \sqrt{1 - y^2}$$

where all of the quantities involved have been defined previously except $C_{L_{\alpha_t}}$ which is the lift-curve slope (per radian) of the trailing wing as determined from reference 21. From the application of strip theory based upon considerations of reversed-flow principles, the roll-influence function for a planar triangular wing (horizontal component of cruciform) is assumed to be given in approximate form by

$$R_A(y) = \left(\frac{l}{q_o \epsilon}\right) y = \frac{2 S_t \, C_{L_{\alpha_t}}}{s_t^2 \pi} \sqrt{1 - y^2} \, y \tag{15}$$

The roll-influence function for the vertical wing component $R_A(z)$ is identical to equation (15) with z substituted for the y variable. The rolling moment on the complete cruciform wing induced by the non-uniform downwash described by equations (6) and (7) is, then, in coefficient form

$$C_{l_t} = \frac{s_t^2}{2 S_t} \left[\int_{-1}^{1} R_A(y) \, \epsilon_h \, dy + \int_{-1}^{1} R_A(z) \, \epsilon_v \, dy \right]$$

Upon substitution for the induced-flow-angle relations and the roll-influence function from equations (6), (7), and (15), this equation becomes

$$C_{l_t} = \frac{\Gamma \, C_{L_{\alpha_t}}}{\pi^2 \, V_o \, s_t} F_A$$

where

$$F_A = \frac{1}{2} \left\{ \int_{-1}^{1} \frac{\sqrt{1-y^2} \, (y-y_1) y \, dy}{(y-y_1)^2 + z_1^2} + \int_{-1}^{1} \frac{\sqrt{1-z^2} \, (z-z_1) z \, dz}{(z_1-z)^2 + y_1^2} \right\}$$

If the value for Γ is substituted in the foregoing expression from equation (12), the final form of the rolling-moment coefficient becomes

$$C_{l_t} = \frac{G \, C_{L_{\alpha_t}} \, S_t}{2\pi^2 \, S_t^2} F_A \tag{16}$$

The integrals in the parameter F_A have been computed and the results are given in the chart presented in figure 6. This chart is similar to those of figure 5 and is designed to be used in the same manner.

Triangular Wings With Leading Edges Swept Well Behind The Mach Cone

In the calculation of the rolling moments induced by an infinite line vortex upon a cruciform wing of triangular plan form with the leading edges of the wing swept well behind the Mach cone, it is not permissible, in general, to neglect the effects of interference between the components of the wing. Reversed-flow principles may be applied to this problem; however, difficulties are encountered in this case because of the fact that the proper roll-influence function to be used in the computations is not obvious. Flow-reversal principles prescribe this function to be the spanwise load distribution for the rolling cruciform wing in reversed flow, for which the solution is unknown. Furthermore, if slenderness approximations are made and it is assumed that the spanwise load distribution for a slender, rolling cruciform wing is that given in reference 2 for either the apex forward or apex rearward wing, the solution is not obtained in closed form. It is necessary, therefore, to consider a more fundamental approach to the problem.

The solution of this problem based on classical hydrodynamical principles is discussed in Appendix B where the rolling-moment coefficient induced by an infinite line vortex on a slender cruciform wing is found to be

$$C_{l_t} = \frac{G}{\pi} F_B \tag{17}$$

In equation (17), G is defined by equation (13) and F_B can be obtained from the chart in figure 7. This chart also is designed to be used in the same manner as those in figures 5 and 6.

APPLICATION OF METHOD AND COMPARISON WITH EXPERIMENTAL RESULTS

In the previous sections methods were proposed for estimating the structure of the downwash field behind lifting wing-body combinations and for determining the rolling moment on a cruciform wing induced by one or more infinite line vortices. By making use of these procedures, it should be possible to estimate the induced-roll characteristics of a missile. In this section this hypothesis will be investigated by comparing experimentally determined rolling moments caused by wing-tail interference with analytical computations for several missiles which differ in design and for which wing-tail interference effects are important. In each case the experimental rolling moments which are presented are caused only by wing-tail interference and, in most cases, were obtained by measuring the difference in the rolling moment on a particular configuration with the trailing wing in place and then removed.

MISSILE A

Experimental data on the induced-rolling-moment characteristics of missile A at 1.4 Mach number were obtained from tests conducted in the Ames 6- by 6-foot supersonic wind tunnel. Pertinent information regarding the apparatus, model, and general procedure for testing the model in this facility can be found in reference 10. Missile A (with the tail in the aft position) differs from the model considered in reference 10 only in that the forward wing panels are reversed about the hinge line. In figure 8, experimentally determined rolling-moment coefficients contributed by the trailing cruciform wing on this model are shown and are compared with computations based upon the theoretical considerations previously presented. The model conditions for which these rolling moments were measured are shown in the sketches included in the figure.

For this model, the leading edges of the trailing wing are sonic at 1.4 Mach number (at least for small angles of attack); therefore, the rolling moment contributed by the trailing wing was computed from equation (14) with m equal to unity. The vortices in the simplified vortex model (see fig. 1) were assumed to originate at the wing trailing edges at 0.5 of the exposed span of each panel (see fig. 9). The vortex strengths were computed from equation (1) by calculating the load on each panel of the cruciform by use of linearized theory with appropriate corrections for wing-body interference obtained from slender-body theory. The effects of sideslip angle upon the vertical wing component were disregarded in these computations; consequently, the vortices from opposing panels of the wing are of equal strength. The paths of the vortices discharged from the forward wing at 12° angle of attack are shown in figure 9. Similar graphical constructions were completed at 4°, 8°, 16°, and 20° angles of attack, and, in figure 10, the location of the vortex cores in the crossflow plane at the center of pressure of the trailing wing (aft position) and portion of the body in combination with this wing are shown for these angles of attack. A few of the lines of constant-rolling-moment parameter (F_1 in eq. (14)) taken from figure 5(d) also are shown in this figure.

In the analysis previously presented for the induced rolling moment on cruciform wings caused by an infinite line vortex, the presence of a body in combination with the wing was not considered. However, ahead of the trailing wing, the effect of the presence of the body was included in estimating the vortex paths, the boundary conditions imposed by the body being satisfied by placing vortex images within the body. At the trailing-wing location, the boundary conditions for the body cannot be handled in such a simple manner. It can be reasoned, however, that if the computations are carried out for the trailing wing (extended to the body center line), the additional considerations required to account for the body are relatively insignificant. In the case of the slender

wing-body combination this question may be examined more rigorously by including the body effect. The procedure outlined in Appendix B for the cruciform, slender wing was repeated for the wing-body case. The resulting expressions were found to be very difficult to evaluate, and, therefore, the results are not included in the method presented in this paper; however, the analysis indicated that the body effect is small provided the body diameter is less than about 0.3[2] of the wing span. It is suggested that for cases where the body diameter is significantly greater than 0.3 of the wing span that a partial correction for the effect of the body may be obtained by considering that the portion of the wing enclosed by the body is ineffective in producing rolling moments. This consideration simply alters the limits of integration in the rolling-moment parameter F (see eqs. (14), (16), and (17)).

For all cases in the examples presented herein, the body diameter of the missiles considered is less than 0.3 of the span of the trailing wing; therefore, the effect of the body is disregarded.

For missile A, then, the rolling-moment parameter F_1 is evaluated from figure 5(d) at each angle of attack for each of the four vortices external to the body shown in figure 10 (the direction of rotation determines the sign of the parameter F_1), and the rolling moment (in coefficient form) contributed by each is computed from equation (14). The total rolling moment on the trailing wing then can be determined by the algebraic addition of the contributions of each of the individual vortices. The results presented in figure 8 show that, except for the interdigitated tail in the aft position, the analytical computations for this missile, for the most part, are in good agreement with the rolling moments obtained experimentally. The discrepancy between theory and experiment for the tail in the aft position (see fig. 8(b) at angles of attack between about 10° and 18°) can be attributed to two causes:

1. The chart in figure 5(d) is drawn for an ideal vortex, whereas in a real fluid, of course, viscosity prescribes that the core velocities be finite. It is believed, therefore, that values of the rolling-moment parameters on this chart obtained for vortex positions coinciding with either of the cruciform-wing components are in error. For the interdigitated configuration under consideration, the vortex discharged from the right horizontal panel of the forward wing passes through the upper right-hand panel of the trailing wing (see fig. 10) in the angle-of-attack range at which the discrepancy between theory and experiment occurs in figure 8(b).

2. From an examination of the charts in figures 5, 6, and 7, it is noted that there is a concentration of lines of constant rolling moment

[2]This value is probably a reasonable guide also for cruciform wing-body combinations which are not slender.

for vortex positions near a wing component (at about 0.7 of the maximum span of the component). It is evident, then, that a small error in estimating the position of a strong vortex in this region can have a large effect upon the contribution of this vortex to the rolling moment. In figure 10 the strong vortex discharged from the right horizontal panel of the forward wing at about 13° angle of attack intersects the upper right-hand panel of the trailing wing at about 0.7 of the span of the panel. Since the position and strength of this vortex are only estimated, the relatively poor agreement between theory and experiment at angles of attack near 13° is believed to be caused by the proximity of this strong vortex to this critical region of the trailing wing.

MISSILE B

Experimental data on the induced-rolling-moment characteristics of missile B at 1.7 Mach number were obtained from reference 22, wherein information regarding the model, apparatus, and procedure for testing the model in the Ames 6- by 6-foot supersonic wind tunnel also may be found. Experimental values of the rolling moment contributed by the cruciform trailing wing situated in the nonuniform downwash field of the forward control surfaces are presented in figure 11. These values were obtained from the results contained in figure 9(a) of reference 22 for the conditions at which the vertical components of the forward control surfaces were deflected 0° and 15°. Rolling-moment data were not available for this model with the trailing wing removed; therefore, the values presented in figure 11 represent not only the wing-tail-interference rolling moments, but also those contributed by the forward control surfaces directly. However, computations, based on the linearized theory of reference 23, indicated that the order of magnitude of these rolling moments (contributed by the forward control surfaces) probably would be within the accuracy of the measurements involved in obtaining the experimental values. For this reason, the rolling moments presented in figure 11 are considered to be caused entirely by wing-tail interference.

The analytical computations (shown in fig. 11) of these induced rolling moments were made from equation (14) by evaluating F_m in this equation from two of the charts in figure 5. Two computations were made because, as will be shown subsequently, the form of the roll-influence function for the trailing wing is not approximated with sufficient accuracy through the angle-of-attack range by any of the roll-influence functions for which the charts in figure 5 were prepared.

To determine F_m, the forward control fins and the body, again, were replaced by the simplified vortex model. The strengths of the vortices were estimated from equation (1) by computing first the lift

on each of the forward control panels as a function of the angle of attack. The lift on the horizontal components was obtained by using the slender-body theory (as applied to rectangular wing-body combinations in ref. 4) in conjunction with the lift-curve slope of the isolated horizontal wing obtained from linearized theory. It is shown in reference 4 that wing-body interference factors based on slender-body theory may be applied to wings of rectangular plan form, provided the aspect ratio of the wing is not large. The lift (or side force) on the vertical-control-surface components was obtained in a similar manner by determining the wing-body interference from slender-body theory as applied (in ref. 24) to rectangular wings deflected with respect to a cylindrical body.

The vortex paths downstream of the forward control surfaces at 12° angle of attack are shown in figure 12. Similar graphical constructions were completed at angles of attack of 4°, 6°, 8°, and 16°. In figure 13, the location of the vortex cores with respect to the trailing wing is shown for these angles of attack. A few of the lines of constant-rolling-moment parameter F_4 taken from figure 5(b) also are shown in this figure.

With the positions of the vortices with respect to the trailing wing determined, the roll-influence function for the independent planar components of this wing was computed from reference 25. This influence function is shown in figure 14 and is compared there with the roll-influence functions given in equation (10). From this comparison, it can be seen that the roll-influence function determined for m equal to 4 in equation (10) most nearly approximates the roll-influence function for the trailing wing at small angles of attack. An examination of figure 13 shows, however, that as the angle of attack increases, the vortices which originate from the forward control surfaces are clustered about the upper vertical component of the trailing wing. The proximity of the vortices to this upper panel requires, therefore, that the roll-influence function for this panel be known fairly accurately, and the approximation given by equation (10) with m equal to 4, which was satisfactory at the lower angles of attack, is probably no longer satisfactory. In line with the same reasoning, it should be noted that, since the vortices in figure 13 are remotely situated with respect to the lower panel of the vertical wing component, the exact roll-influence function for the lower panel at large angles of attack is of secondary importance in comparison to that for the upper panel. Furthermore, with reference to sketch (a), it can be seen that the Mach wave from the tip of the upper wing panel approaches the wing tip as the model angle of attack increases. Another effect of increasing the angle of attack of the model, therefore, is to increase the spanwise loading near the tip of the upper panel of the vertical wing component. A precise determination of the roll-influence function in the vicinity of the tip of the upper panel was not carried out. This function was estimated to vary with

angle of attack of the model in such a manner as to permit the influence function for the complete wing to be represented at low angles of attack by equation (10) with m equal to 4, and at large angles of attack by the same equation with m equal to infinity.

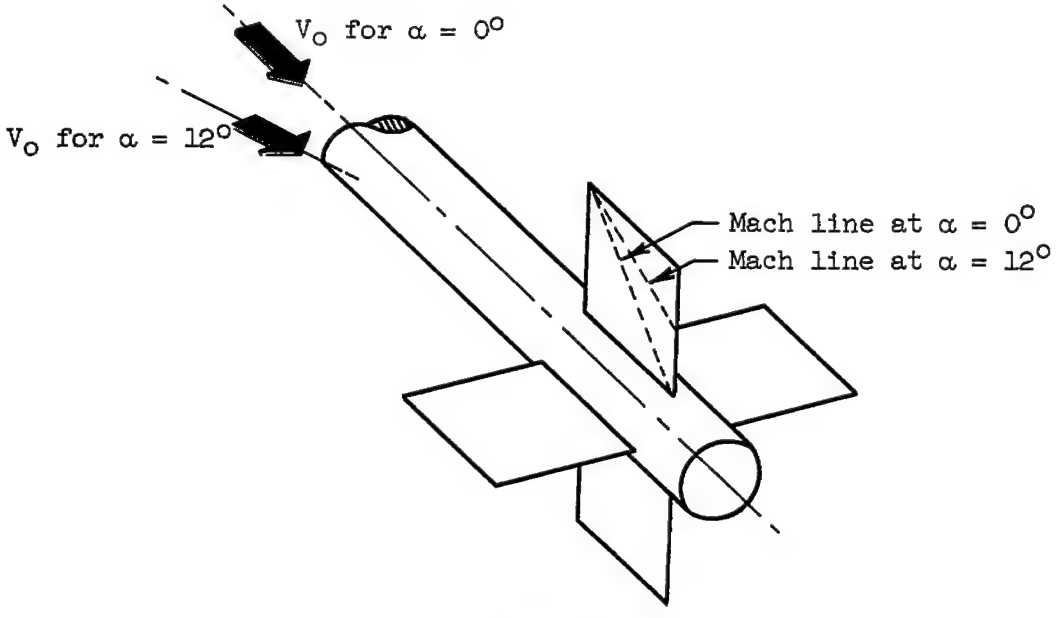

Sketch (a).

In accordance with these considerations, the rolling moment contributed by each of the four vortices external to the body in figure 13 was determined from equation (14) by evaluating the rolling-moment parameter F_m from charts 5(a) and 5(b). The results are shown in figure 11. The experimental values are close to the predicted values based on the rolling-moment parameter F_4 at lower angles of attack. As the angle of attack increases, the rolling moment is more nearly predicted by the curve based upon the assumption that the planar components of the trailing wing can be represented by high-aspect-ratio rectangular wings placed at right angles to one another. Thus, the approximations seem to be justified by the experimental results to an angle of attack of about 12^o. As the angle of attack increases above 12^o, the agreement deteriorates. The failure of the calculations to predict the rolling moment at angles of attack greater than about 12^o is believed to result from the formation of additional vortices caused by viscous separation of the crossflow about the body downstream of the forward control fins. In contrast to missile A, the possibility of viscous separation of the body crossflow is an important consideration for this missile at large angles of attack for two reasons:

1. The major portion of the lift is contributed by the trailing wing; consequently, the downwash from the forward lifting surfaces is not sufficient to suppress completely the effects of viscosity in the crossflow about the body downstream of the forward control fins.

2. The distance between the control-fin trailing edges and the trailing wing is large, and, therefore, an appreciable portion of the lift of the missile at large angles of attack is contributed by this part of the body.

It is recalled that in the graphical constructions, the induced effects of the body on the paths of the vortices downstream of the control fins were computed by assuming that the crossflow about the body could be represented by the two-dimensional, inviscid flow about an infinite circular cylinder. For this particular missile, however, it is probable that the crossflow about the body changes progressively with angle of attack of the missile in the manner shown schematically in sketch (b).

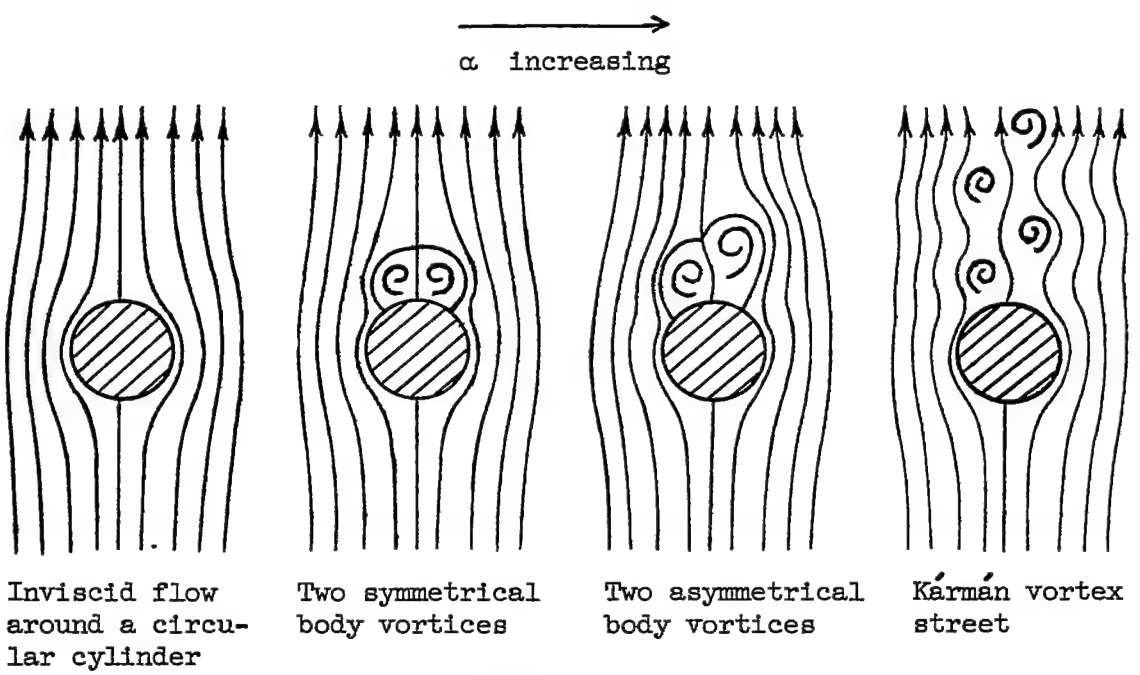

Sketch (b).

The flow about inclined bodies of revolution is discussed at some length in references 15 and 16, wherein the effects of viscous separation of the flow about such bodies are shown to be significant. In

many cases during the investigations reported in reference 16, flows of the type indicated in the accompanying sketch were observed by means of water-tank and vapor-screen techniques. Neither the body angles of attack to which each of these flows might correspond for the present missile nor the locations of the body vortices and their strengths can be determined at the present time. It is known, however, that the strengths of these vortices, in flows involving two body vortices, increase with increasing distance downstream. Rough estimates at 16° angle of attack of the strengths of the vortices which could originate from the body of missile B indicated that in the vicinity of the trailing wing, they could be of the same order of magnitude as those which originate from the forward control fins.

For angles of attack between 0° and about 14°, it is believed that the crossflow about the body of the missile is of the type characterized by 1 and 2 in sketch (b). The symmetrical pair of vortices do not contribute to the rolling moment, of course, but will have a small effect upon the paths of the vortices that originate at the forward control fins. There are strong indications, however, that the flow is of type 3 for higher angles of attack and that the major portion of the rolling moment in this range is contributed by the asymmetrical body vortices. The formation of a vortex street within the angle-of-attack range for which rolling-moment data for this missile were available seems unlikely since the results of reference 16 indicate that, in general, this transition takes place at considerably higher angles of attack. Furthermore, the formation of a vortex street probably would be accompanied by erratic unsteady rolling moments (of the type discussed in ref. 26) which were not noted in the results presented in reference 22. If the location and strengths of the body vortices could be determined, they could be included in the graphical constructions carried out in the present analysis to determine the downwash structure in the region of the trailing wing; and, more accurate estimates of the rolling moment at large angles of attack could be made. Further research on this phase of the problem is required, however.

MISSILE C

Missile C (with the tail in the aft position) is identical to the model described in reference 10 and differs from missile A only in that the forward wing panels are reversed about the hinge line. The experimental values of the induced rolling moments presented in figure 15 were obtained in the Ames 6- by 6-foot supersonic wind tunnel. The model conditions for which these rolling moments were measured are shown in the sketch included in the figure. These rolling moments were obtained from measurements with the tail in place by subtracting from these values the rolling moment on the model with the tail removed.

Initial computations of the induced rolling moments for this model were performed in exactly the same manner as for the two missiles previously discussed. The cruciform forward wing was treated as two independent, planar wing-body combinations, having a lift (or side force) given by linear theory with suitable corrections for wing-body interference obtained from slender-body theory. The vortex centers of gravity were considered to be at 0.8 of the panel spans. Diametrically opposed vortices again were considered to be of equal strength. Graphical computations of the vortex motions were carried out at 4° intervals in angle of attack, and the rolling moment contributed by the tail in the aft position was computed from equation (14). The results of these computations are shown by the broken line in figure 15. The computed values, in general, predict the variation of the experimental rolling moments with angle of attack; however, the magnitude is not predicted. From this result, it was considered advisable to investigate the division of the loading on the forward wing panels to ascertain, insofar as possible, the effect of sideslip angle upon the vertical component of the cruciform wing (see footnote 1, p. 6).

In figures 16(a) and 16(b) are shown the measured loads for one of the triangular-wing panels of missile C mounted on the body in the presence and absence of the other three panels of the cruciform wing. Examination of these results indicates that throughout most of the range of angles of attack and angles of sideslip investigated, the total lift of an isolated panel is not changed significantly by the presence of the other three panels. Computed values of the total lift on each panel are shown by the solid lines in figure 16 and were calculated by the method proposed in reference 10. The lift on a panel is obtained as the lift on one half of the planar wing formed by joining the panel to the diametrically opposed panel of the cruciform configuration and by making corrections for wing-body interference dependent upon wing-span-body-diameter ratio in accordance with slender-body theory. This calculation applied to the triangular panels of missile C results in the panel loadings being markedly influenced by the sideslip angle. Computations of the panel lifts by this procedure are in good agreement with the experimental results.

On the basis of the previously discussed independency of the panel lifts on the forward wing of missile C, it is assumed (in accordance with eq. (1)) that this independence applies also to the discharged vorticity from opposing panels of the wing. Accordingly, computations of the tail rolling moments were performed for the theoretical values of the lifts on panels 2 and 4 (shown in figure 16(a)) related to the vortex strengths discharged from these panels by means of equation (1). The strengths of the vortices discharged from the horizontal components of the wing remained unchanged from the values used in the previous computations. The locations of the vortex centers of gravity also remained unchanged at the 0.8-panel-span position. The paths of these

[redacted]

vortices trailing downstream of the wing at 12° angle of attack are shown in figure 17. The location of the vortex cores in the crossflow plane at the center of pressure of the tail (aft position) and portion of the body in combination with the tail are shown in figure 18 for 4° increments in angle of attack. Again, a few of the lines of constant rolling-moment parameter F_1 (eq. (14)) obtained from figure 5(d) are presented in this figure. In figure 15, computed rolling moments are shown for both interdigitated and in-line tails at two positions behind the wing. The results appear to indicate that this modified computation more nearly agrees with the experimental values than the previous computation which assumed that vortices of equal strength are discharged from opposing panels of the wing in accordance with linear theory. The reasons for the discrepancy between theory and experiment at angles of attack between 10° and 18° for the interdigitated tail in the aft position (see fig. 15(b)) are believed to be the same as those discussed for missile A with the tail in the same position.

MISSILE D

Experimental data on the induced-rolling-moment characteristics of missile D at 1.72 Mach number were obtained from tests conducted in the bomb tunnel at Aberdeen Proving Ground, Maryland, as reported in reference 27. The experimental results given in figure 71 of that report are typical of the nonlinear variations of rolling moment with angle of attack which are considered in this report.

Measured values of the rolling moments for this missile caused by wing-tail interference, for the condition in which the vertical components of the forward control fins are deflected 10° with respect to the body center line, are shown in figure 19. These values were obtained from figure 71 of reference 27 by subtracting the rolling moments measured with the forward wings undeflected from those measured with the vertical components of the forward control fins deflected 10°. Unfortunately, the data in reference 27 are incomplete in that the rolling moments on the model with the trailing wing removed are not presented. The rolling moment contributed by the forward control fins is believed, however, to be small, and their contribution to the rolling moment has been neglected in the present analysis.

Upon consideration of the aspect ratio of the trailing wing and the Mach number, it was concluded that the rolling moment probably would be most accurately predicted by equation (16). To determine F_A in equation (16) from the chart in figure 6, the forward control surfaces and the body were replaced by the simplified vortex system shown in figure 1. The strengths of these vortices were computed from equation (1) by determining the division of lift on the forward control fins in a similar

manner to that of the modified computation performed for missile C. In the crossflow plane at the trailing edge of the forward control fins, the spanwise positions of the vortex-sheet centers of gravity were estimated to be at 0.8 of the exposed maximum semispan of each panel. Because of the sweep angle of these fins, however, progressive rolling up of the vortex sheet ahead of the control-fin trailing edge was believed to exert some influence on the positions of the vortex-sheet centers of gravity normal to the fin chord planes. As a rough approximation of this displacement, the vortices were assumed to leave the wing at the hinge line of each panel. (Subsequent computations, in which the trailing vortices were assumed to originate on the control surface trailing edge, produced essentially the same results as shown in figure 19.) The paths of the vortices external to the body and of the image vortices at 12° angle of attack are shown in figure 20. Similar graphical constructions were completed at 4° increments in angle of attack. In figure 21, the locations of the vortex cores with respect to the trailing wing are shown for these angles of attack, and lines of constant rolling-moment parameter F_A taken from figure 6 also are shown. In these graphical constructions, the body behind the control-fin trailing edges (see fig. 20) was assumed to be of constant diameter equal to the diameter of the cylindrical portion of the body in the vicinity of the trailing wing.

As stated previously, the rolling moment contributed by each of the four vortices external to the body was computed by use of equation (16). The results presented in figure 19 indicate that the analytical computations agree fairly well with the experimental results for angles of attack between 0° and about 14°. For larger values of angle of attack, the discrepancy between theory and experiment is believed to be caused by viscous separation of the crossflow about the body downstream of the forward control fins. This effect was discussed in connection with the experimental and analytical results for missile B. It is interesting to note the correspondence between the rolling moments, at large angles of attack, for missiles B and D and two similarities in their design; namely,

1. Both are canard arrangements in which the ratio of the body diameter to the span of the forward wing is relatively large.

2. In each case, the distance between the forward wing and the trailing wing is large.

Because of these similarities, the effects of the body crossflow mentioned previously in the discussion of the results for missile B are considered to apply as well for missile D.

CONCLUDING REMARKS

The analytical portions of this report relate the aerodynamic and geometric considerations involved in determining wing-tail-interference effects for missiles. Although particular attention is focused upon the induced rolling-moment problem, the induced lift and its resultant effect upon the longitudinal stability of missiles could be handled in an analogous manner.

Although the method used in this report involves a number of assumptions, it succeeds in estimating the induced-roll effects for a number of missile configurations with surprising accuracy. Undoubtedly, the precision with which these effects can be estimated will improve with a more complete understanding of the manner in which vorticity is discharged from the forward lifting elements of tandem-wing airframes. In any event, the roll-influence charts provided in the report should be useful in quickly estimating the rolling moment contributed by any vortex system once it has been established.

Ames Aeronautical Laboratory
National Advisory Committee for Aeronautics
Moffett Field, Calif., Aug. 18, 1953

APPENDIX A

DETAILS OF THE GRAPHICAL PROCEDURE

In order to explain the manner in which the charts in figure 2 are used in determining the paths of the vortices downstream of the simplified model of the lifting cruciform wing-body combination, each step in the procedure is itemized as follows:

1. The circular cross section of the body of the missile is drawn on tracing paper and scaled to fit exactly the diameter of the half circle shown in figure 2(b). It should be noted that the chart sizes shown in figure 2 are not large enough to give sufficient accuracy for most purposes. A circle diameter of approximately 5 inches has been found to be convenient.

2. The locations of the vortices at the wing trailing edges are determined in accordance with the assumptions involved in constructing the simplified model which were discussed within the body of the report. The direction of rotation and the value of the strength parameter B (see eq. (4)) are noted beside each vortex.

3. The positions of the image vortices are determined from chart I in figure 2(a) which is a plot of the relationship given in equation (5). The value of B for each of the image vortices is the same as for its companion vortex outside the body; however, the direction of rotation is reversed.

4. With the position of the vortices in the crossflow plane at the wing trailing edge noted, a step-by-step procedure is begun to determine the deflection of each vortex in the time interval, t, caused by the presence of the remaining seven vortices and the body crossflow. For vortex number 1 the crossflow direction and crossflow factor, k, are determined from chart II in figure 2(b). With this value of k, the deflection distance is picked from chart III in figure 2(a) for the appropriate value of the crossflow parameter $l_t/Kd \sin \alpha$.

5. With chart IV of figure 2(a) as the underlay, the center of vortex number 2 is placed at the origin with vortex number 1 on the horizontal axis. The deflection distance corresponding to the value of B for vortex number 2 is determined from the lines of constant values of the strength parameter B shown in chart IV. This vector, then, is added to the crossflow vector determined in step 4. This process is repeated for the influence of vortices 3 and 4 and the four image vortices on the position of vortex 1. The end point of the last vector determines the new position of vortex 1 at the end of the first time interval.

[redacted]

6. The foregoing steps are repeated for each of the vortices in the flow field external to the body in order to find the position of these vortices at the end of the first interval. The locations of the image vortices within the body at the end of this time interval are determined from the new positions of the vortices external to the body by using chart I as an underlay.

7. With the positions of the vortices at the end of the first interval determined, an identical procedure is carried out to find the positions of the vortices at the end of the second and succeeding intervals until the vortex positions are found at the end of the tenth interval, corresponding to the position downstream of the wing at which the structure of the downwash field is desired.

8. With the orientation of the vortices with respect to the trailing wing approximated in accordance with the foregoing procedure and subject, of course, to the consideration that this wing is one of the types for which equations (14), (16), and (17) were derived, the induced rolling moment can be computed by appropriately choosing between these equations.

APPENDIX B

ROLLING MOMENT OF A SLENDER TRIANGULAR WING (CRUCIFORM) IN THE PRESENCE OF AN INFINITE LINE VORTEX

General Considerations

The linearized partial differential equation for the perturbation velocity potential φ' in subsonic or supersonic flow is

$$(1 - M_o^2)\,\varphi'_{xx} + \varphi'_{yy} + \varphi'_{zz} = 0 \tag{B1}$$

where the free stream is directed parallel to the positive x axis (see sketch (c)). The present analysis is concerned with the determination of the

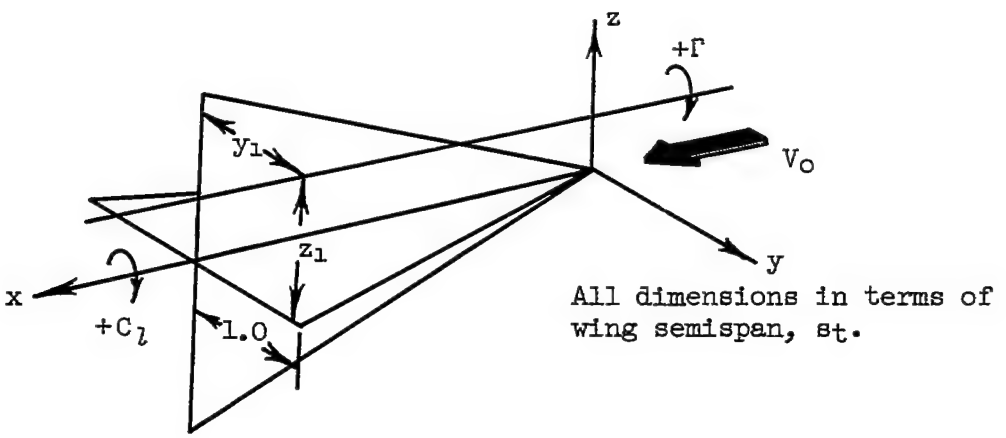

Sketch (c).

rolling moment on the basis of the slender-wing approximation which reduces equation (B1) to the Laplace equation in two dimensions. The problem will be treated by well-known methods of slender-wing theory as introduced by Jones (ref. 28) and extended by others.

The problem is solved by finding a solution to Laplace's equation

$$\varphi'_{yy} + \varphi'_{zz} = 0 \tag{B2}$$

which satisfies the following boundary conditions:

1. Perturbation velocities vanish at infinity.

2. The velocity potential is continuous at all points in space, except across the wing surfaces.

3. The velocity components Φ_y' and Φ_z' are continuous everywhere in space.

4. At all points which are to represent the surface of the wing, the normal components of velocity are specified.

By use of methods of classical hydrodynamics and, in particular, the methods of conformal transformation, a potential function that satisfies the boundary conditions stated above can be found from which the rolling moments induced by an infinite line vortex on a slender cruciform wing can be determined.

Theoretical Analysis

An equation which transforms the region outside a rotationally symmetric cross in the X plane into the region outside a circle of radius s_1 in the σ plane (see sketch (d)) was obtained in reference 2 as

$$2X^2 = \sigma^2 + \frac{s_1^4}{\sigma^2} \tag{B3}$$

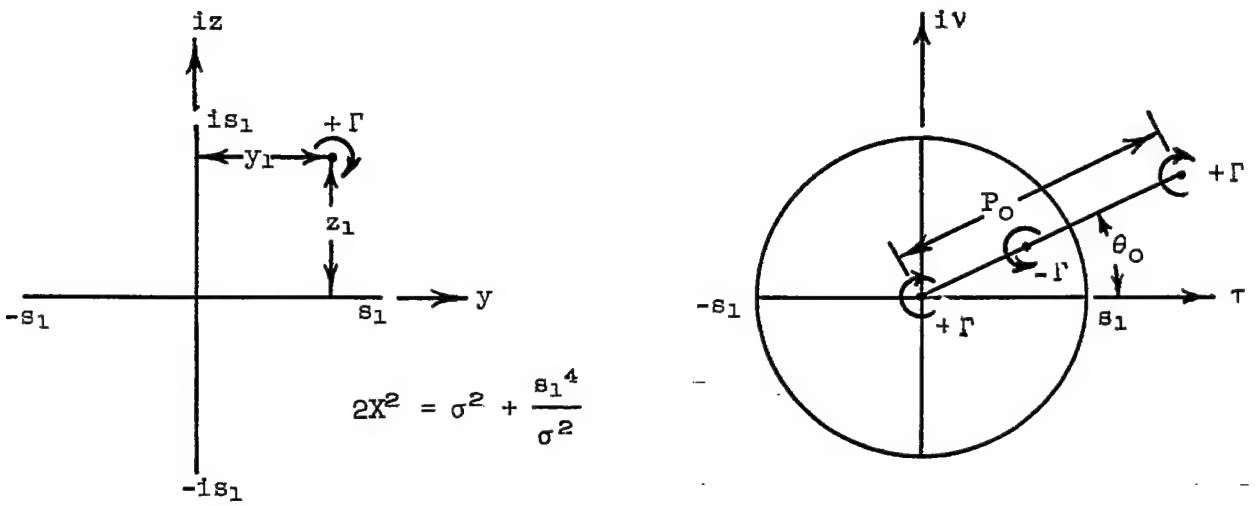

(a) X plane (b) σ plane

Sketch (d).

[redacted]

This equation transforms the circumference of the circle ($\sigma = s_1 e^{i\theta}$) in the σ plane into the cross of width $2s_1$, in the X plane as is shown in the sketch.

If a two-dimensional vortex of strength Γ is located at the point ($\sigma_o = P_o e^{i\theta_o}$) outside the circle in the σ plane, the image system inside the circle consists of a vortex of strength $-\Gamma$ at the inverse point ($\sigma_1 = s_1^2/\bar{\sigma}_o$ where $\bar{\sigma}_o = P_o e^{-i\theta_o}$) and a vortex of strength Γ located at the center of the circle (see ref. 29, p. 326). The flow in the σ plane may be transformed to the X plane by means of equation (B3) and results in a two-dimensional flow about a cruciform lamina in the presence of a single external vortex. In the circle plane the complex potential for the vortex in the presence of the circle is

$$\Phi = \frac{i\Gamma}{2\pi} \log (\sigma - \sigma_o) - \frac{i\Gamma}{2\pi} \log (\sigma - \sigma_1) + \frac{i\Gamma}{2\pi} \log \sigma \tag{B4}$$

where

$\sigma = s_1 e^{i\theta}$ (s_1 is in terms of the semispan s_t)

$\sigma_o = P_o e^{i\theta_o}$ (P_o is in terms of the semispan s_t)

$\sigma_1 = (s_1^2/P_o) e^{i\theta_o}$

From equation (B4) and the transformation equation (B3), a two-dimensional velocity potential which satisfies the boundary conditions for the flow in the X plane may be obtained from which the loading[3] on the cruciform wing may be written as

$$\frac{\Delta p}{q_o} = \frac{2}{V_o} \Delta \left(\frac{\partial \varphi'}{\partial x} \right) \tag{B5}$$

where φ' is the velocity potential in the plane of the cross. The expression for the pressure coefficient given in equation (B5) may be integrated over half of the slender cruciform wing in the $z = 0$ plane to obtain the rolling moment on one panel as

$$L_t' = -\rho_o V_o \int_o^1 \int_{LE}^{TE} \Delta \left(\frac{\partial \varphi'}{\partial x} \right) dx\, y\, dy$$

$$= -\rho_o V_o \int_o^1 \left(\Delta \varphi'_{TE} - \Delta \varphi'_{LE} \right) y\, dy \tag{B6}$$

[3]Squared terms in the expression for the pressure coefficient are disregarded throughout this analysis.

where the subscripts refer to the trailing and leading edges of the wing. Equation (B6) may be transformed by means of equation (B3) to give the rolling moment in the σ plane as

$$L_t' = \rho_o V_o \, s_1^2 \int_{-\pi/4}^{\pi/4} (\varphi_{TE} - \varphi_{LE}) \sin 2\theta \, d\theta \tag{B7}$$

From equation (B4), the velocity potential in the plane of the circle is

$$\varphi = \frac{\Gamma}{2\pi} \left\{ -\tan^{-1} \left(\frac{s_1 \sin\theta - P_o \sin\theta_o}{s_1 \cos\theta - P_o \cos\theta_o} \right) + \tan^{-1} \left[\frac{s_1 \sin\theta - (1/P_o)\sin\theta_o}{s_1 \cos\theta - (1/P_o)\cos\theta_o} \right] - \theta \right\} \tag{B8}$$

The total rolling moment on the cruciform wing may be determined from equations (B7) and (B8) and may be expressed as

$$L_t' = \frac{\rho_o V_o \, \Gamma \, s_t^2}{2\pi} F_B \tag{B9}$$

where

$$\left(\frac{\Gamma}{\pi}\right) F_B = \int_{-\pi/4}^{\pi/4} \varphi \sin 2\theta d\theta - \int_{\pi/4}^{3\pi/4} \varphi \sin 2\theta d\theta + \int_{3\pi/4}^{5\pi/4} \varphi \sin 2\theta d\theta - \int_{5\pi/4}^{7\pi/4} \varphi \sin 2\theta d\theta$$

The rolling moment given in equation (B9) may be related to the simplified model of the lifting, cruciform wing-body combination developed within the body of the report by substituting for Γ from equation (12). With this substitution, the expression for the rolling-moment coefficient is

$$C_{l_t} = \frac{G}{\pi} F_B \tag{B10}$$

The integrals in the parameter F_B have been evaluated for various positions of a line vortex in the σ plane and transformed to the X plane. In figure 8, a chart showing constant values of the parameter F_B is given. From this chart, the rolling-moment coefficient (given in eq. (B10)) for slender, cruciform wings of triangular plan form induced by one or more line vortices may be determined. From symmetry, the rolling moment contributed by vortices located in other quadrants with respect to the wing also can be determined from this chart.

REFERENCES

1. Spreiter, John R.: The Aerodynamic Forces on Slender Plane- and Cruciform-Wing and Body Combinations. NACA Rep. 962, 1950. (Formerly NACA TN's 1662 and 1897.)

2. Adams, Gaynor J., and Dugan, Duane W.: Theoretical Damping in Roll and Rolling Moment Due to Differential Wing Incidence for Slender Cruciform Wings and Wing-Body Combinations. NACA Rep. 1088, 1952. (Formerly NACA TN 2270.)

3. Ferrari, Carlo: Interference Between Wing and Body at Supersonic Speeds - Theory and Numerical Application. Jour. Aero. Sci., vol. 15, no. 6, June 1948, pp. 317-336.

4. Nielsen, Jack N., and Pitts, William C.: Wing-Body Interference at Supersonic Speeds With an Application to Combinations With Rectangular Wings. NACA TN 2677, 1952.

5. Lagerstrom, Paco A., and Graham, Martha E.: Aerodynamic Interference in Supersonic Missiles. Douglas Aircraft Co., Rep. SM-13743, July 1950.

6. Stewart, Homer J., and Meghreblian, Robert V.: Body-Wing Interference in Supersonic Flow. GALCIT/JPL PR 4-99, June 1949.

7. Nielsen, Jack N., Katzen, Elliott D., and Tang, Kenneth K.: Lift and Pitching-Moment Interference Between a Pointed Cylindrical Body and Triangular Wings of Various Aspect Ratios at Mach Numbers of 1.50 and 2.02. NACA RM A50F06, 1950.

8. Nielsen, Jack N., and Kaattari, George E.: Method for Estimating Lift Interference of Wing-Body Combinations at Supersonic Speeds. NACA RM A51J04, 1951.

9. Cramer, R. H.: Interference Between Wing and Body at Supersonic Speeds, Part V - Phase I Wind Tunnel Tests Correlated With the Linear Theory, Cornell Aeronautical Laboratory Rep. CM - 597, Oct. 1950.

10. Edwards, S. Sherman: Experimental and Theoretical Study of Factors Influencing the Longitudinal Stability of an Air-to-Air Missile at a Mach Number of 1.4. NACA RM A51J19, 1952.

11. Spahr, J. Richard, and Dickey, Robert R.: Wind-Tunnel Investigation of the Vortex Wake and Downwash Field Behind Triangular Wings and Wing-Body Combinations at Supersonic Speeds. NACA RM A53D10, 1953.

12. Wetzel, Benton E., and Pfyl, Frank A.: Measurements of Downwash and Sidewash Behind Cruciform Triangular Wings at Mach Number 1.4. NACA RM A51B20, 1951.

13. Spreiter, John R., and Sacks, Alvin H.: The Rolling Up of the Trailing Vortex Sheet and Its Effect on the Downwash Behind Wings. Jour. Aero. Sci., vol. 18, no. 1, Jan. 1951.

14. Bird, John D.: Visualization of Flow Fields by Use of a Tuft Grid Technique. Jour. Aero. Sci., vol. 19, no. 7, July 1952.

15. Allen, H. Julian: Estimation of the Forces and Moments Acting on Inclined Bodies of Revolution of High Fineness Ratio. NACA RM A9I26, 1949.

16. Allen, H. Julian, and Perkins, Edward W.: Characteristics of Flow Over Inclined Bodies of Revolution. NACA RM A50L07, 1951.

17. Lin, C. C.: On the Motion of Vortices in Two Dimensions. Appl. Math., series no. 5, Univ. Toronto Press, Toronto, Canada, 1943.

18. Heaslet, Max. A., and Lomax, Harvard: The Calculation of Downwash Behind Supersonic Wings With an Application to Triangular Plan Forms. NACA Rep. 957, 1950. (Formerly NACA TN's 1620 and 1803.)

19. Heaslet, Max. A., and Spreiter, John R.: Reciprocity Relations in Aerodynamics. NACA TN 2700, 1952.

20. Alden, Henry Leonard, and Schindel, Leon H.: The Calculation of Wing Lift and Moments in Nonuniform Supersonic Flows. M.I.T. Meteor Rep. No. 53, May 1950.

21. Brown, Clinton E.: Theoretical Lift and Drag of Thin Triangular Wings at Supersonic Speeds. NACA TN 1183, 1946.

22. Chubb, Robert S.: Experimental Investigation of the Stability, Control and Induced Rolling Moments of a Canard Missile Airframe at a Mach Number of 1.7. NACA RM A52G29, 1952.

23. Jones, Arthur L., Spreiter, John R., and Alksne, Alberta: The Rolling Moment Due to Sideslip of Triangular, Trapezoidal, and Related Plan Forms in Supersonic Flow. NACA TN 1700, 1948.

24. Nielsen, Jack N., Kaattari, George E., and Drake, William C.: Comparison Between Prediction and Experiment for All-Movable Wing and Body Combinations at Supersonic Speeds - Lift, Pitching Moment, and Hinge Moment. NACA RM A52D29, 1952.

25. Harmon, Sidney M.: Stability Derivatives of Thin Rectangular Wings at Supersonic Speeds. Wing Diagonals Ahead of Tip Mach Lines. NACA TN 1706, 1948.

26. Mead, Merrill H.: Observations of Unsteady Flow Phenomena for an Inclined Body Fitted with Stabilizing Fins. NACA RM A51K05, 1952.

27. Fischer, H. S.: Data Report on Supersonic Wind-Tunnel Tests of a 0.075-Scale Model of the Nike 484 Missile. Douglas Aircraft Co. Rep. SM-14015, June 1951.

28. Jones, Robert T.: Properties of Low-Aspect-Ratio Pointed Wings at Speeds Below and Above the Speed of Sound. NACA TN 1032, 1946.

29. Milne-Thomson, L. M.: Theoretical Hydrodynamics, 2nd ed. The MacMillan Co., New York, 1950.

[redacted]

TABLE I.- TABULATED VALUES OF THE PARAMETERS NECESSARY TO REPRODUCE THE CHARTS IN FIGURE 2(a)

(a) Chart I

$\frac{f}{d}$	$\frac{e}{d}$
0.5	0.5000
.6	.4160
.8	.3125
1.0	.2500
1.2	.2083
1.4	.1786
1.6	.1563
1.8	.1389
2.0	.1250
2.2	.1136
2.4	.1042
2.6	.0962
2.8	.0893
3.0	.0833
3.2	.0781
3.4	.0735
3.6	.0694
3.8	.0658
4.0	.0625
4.2	.0595
4.4	.0568
4.6	.0543
4.8	.0521
5.0	.0500

(b) Chart III

k	$\frac{hCF}{d}$			
	D = 0.1	D = 0.5	D = 1.0	D = 1.5
0.6	0.06	0.30	0.60	0.90
.7	.07	.35	.70	1.05
.8	.08	.40	.80	1.20
.9	.09	.45	.90	1.35
1.0	.10	.50	1.00	1.50
1.1	.11	.55	1.10	1.65
1.2	.12	.60	1.20	1.80
1.3	.13	.65	1.30	1.95
1.4	.14	.70	1.40	2.10
1.5	.15	.75	1.50	2.25
1.6	.16	.80	1.60	2.40
1.7	.17	.85	1.70	2.55
1.8	.18	.90	1.80	2.70
1.9	.19	.95	1.90	2.85
2.0	.20	1.00	2.00	3.00

Where:

$$D = \frac{l_t}{Kd} \sin \alpha$$

TABLE I.- TABULATED VALUES OF THE PARAMETERS NECESSARY TO REPRODUCE THE CHARTS IN FIGURE 2(a) - Concluded

(c) Chart IV

$\frac{r'}{d}$	$\frac{hr_n}{d}$											
	B=0.02	B=0.04	B=0.06	B=0.08	B=0.10	B=0.12	B=0.14	B=0.16	B=0.18	B=0.20	B=0.22	B=0.24
0.5	0.0400	0.080	0.120	0.160	0.200	0.240	0.280	0.320	0.360	0.400	0.440	0.480
1.0	.0200	.040	.060	.080	.100	.120	.140	.160	.180	.200	.220	.240
1.5	.0130	.027	.040	.053	.067	.080	.093	.107	.120	.133	.147	.160
2.0	.0100	.020	.030	.040	.050	.060	.070	.080	.090	.100	.110	.120
2.5	.0080	.016	.024	.032	.040	.048	.056	.064	.072	.080	.088	.096
3.0	.0070	.013	.020	.027	.033	.040	.047	.053	.060	.067	.073	.080
3.5	.0060	.011	.017	.023	.029	.034	.040	.046	.051	.057	.063	.069
4.0	.0050	.010	.015	.020	.025	.030	.035	.040	.045	.050	.055	.060
4.5	.0045	.009	.013	.018	.022	.027	.031	.036	.040	.044	.049	.053
5.0	.0040	.008	.012	.016	.020	.024	.028	.032	.036	.040	.044	.048
5.5	.0035	.0075	.011	.015	.018	.022	.025	.029	.033	.036	.040	.044
6.0	.0030	.0070	.010	.013	.017	.020	.023	.027	.030	.033	.037	.040

TABLE II.- TABULATED VALUES OF THE PARAMETERS NECESSARY TO REPRODUCE CHART II IN FIGURE 2(b)

(a) Streamlines

$\frac{z'}{d}$	$\frac{y'}{d}$	$\frac{z'}{d}$	$\frac{y'}{d}$	$\frac{z'}{d}$	$\frac{y'}{d}$	$\frac{z'}{d}$	$\frac{y'}{d}$	$\frac{z'}{d}$	$\frac{y'}{d}$	$\frac{z'}{d}$	$\frac{y'}{d}$	$\frac{z'}{d}$	$\frac{y'}{d}$	$\frac{z'}{d}$	$\frac{y'}{d}$
0	0.5500	0	0.6000	0	0.7000	0	0.8000	0	0.9000	0	1.0000	0	1.1000		
.0480	.5481	.0524	.5980	.0611	.6982	.0685	.7983	.0986	.8984	.0874	.9985	.0961	1.0986		
.0957	.5424	.1045	.5925	.1222	.6928	.1399	.7932	.1576	.8936	.1753	.9940	.1930	1.0943		
.1429	.5331	.1563	.5835	.1833	.6840	.2103	.7848	.2373	.8856	.2643	.9865	.2914	1.0873		
.1893	.5200	.2076	.5705	.2444	.6716	.2814	.7731	.3184	.8746	.3553	.9762	.3922	1.0776		
.2348	.5034	.2684	.5540	.3059	.6560	.3536	.7583	.4014	.8608	.4492	.9632	.4969	1.0655		
.2791	.4834	.3085	.5343	.3679	.6372	.4277	.7407	.4875	.8443	.5473	.9479	.6069	1.0511		
.3222	.4601	.3581	.5115	.4310	.6155	.5044	.7204	.5780	.8255	.6514	.9303	.7246	1.0349		
.3640	.4337	.4074	.4855	.4960	.5911	.5855	.6978	.6751	.8046	.7645	.9111	.8534	1.0170		
.4045	.4045	.4569	.4570	.5644	.5644	.6732	.6732	.7821	.7821	.8904	.8904	.9980	.9980		
.4441	.3727	.5076	.4260	.6384	.5357	.7712	.6472	.9039	.7585	1.0355	.8689	1.1659	.9783		
.4834	.3385	.5609	.3930	.7220	.5056	.8856	.6202	1.0486	.7343	1.2098	.8471	1.3689	.9586		
.5235	.3023	.6200	.3580	.8220	.4746	1.0270	.5929	1.2302	.7103	1.4302	.8257	1.6269	.9393		
.5670	.2644	.6906	.3220	.9512	.4436	1.2146	.5664	1.4737	.6872	1.7273	.8055	1.9756	.9212		
.6190	.2253	.7850	.2855	1.1363	.4136	1.4878	.5415	1.8886	.6661	2.1627	.7872	2.4866	.9051		
.6929	.1857	.9340	.2505	1.4414	.3862	1.9397	.5197	2.4186	.6481	2.8801	.7717	3.3272	.8915		
.8326	.1468	1.2359	.2180	2.0634	.3637	2.8498	.5025	3.5962	.6341	4.3096	.7599	4.9980	.8813		
1.2843	.1124	2.2078	.1930	3.9810	.3483	5.6160	.4914								
0	1.2000	0	1.3000	0	1.4000	0	1.5000	0	1.6000	0	1.7000	0	1.8000		
.1049	1.1987	.1137	1.2987	.1224	1.3988	.1312	1.4989	.1399	1.5989	.1487	1.6990	.1574	1.7990		
.2107	1.1946	.2284	1.2950	.2460	1.3953	.2637	1.4955	.2814	1.5957	.2991	1.6960	.3167	1.7961		
.3133	1.1880	.3453	1.2887	.3723	1.3894	.3992	1.4899	.4262	1.5904	.4531	1.6909	.4800	1.7913		
.4292	1.1792	.4660	1.2802	.5028	1.3813	.5395	1.4823	.5763	1.5832	.6130	1.6840	.6496	1.7848		
.5445	1.1676	.5920	1.2695	.6394	1.3712	.6868	1.4728	.7341	1.5742	.7813	1.6768	.8285	1.7767		
.6664	1.1541	.7257	1.2569	.7849	1.3594	.8439	1.4617	.9028	1.5637	.9619	1.6655	1.0203	1.7672		
.7975	1.1390	.8702	1.2427	.9426	1.3461	1.0147	1.4491	1.0866	1.5519	1.1584	1.6544	1.2300	1.7567		
.9418	1.1224	1.0298	1.2273	1.1174	1.3316	1.2046	1.4355	1.2915	1.5391	1.3781	1.6423	1.4644	1.7452		
1.1048	1.1048	1.2109	1.2109	1.3164	1.3164	1.4213	1.4213	1.5257	1.5257	1.6297	1.6297	1.7332	1.7332		
1.2951	1.0868	1.4232	1.1942	1.5503	1.3009	1.6765	1.4068	1.8020	1.5121	1.9269	1.6169	2.0512	1.7212		
1.5262	1.0687	1.6817	1.1776	1.8358	1.2854	1.9886	1.3924	2.1403	1.4987	2.2911	1.6092	2.4411	1.7093		
1.8206	1.0512	2.0118	1.1615	2.2008	1.2707	2.3877	1.3787	2.5735	1.4858	2.7578	1.5922	2.4409	1.6980		
2.2192	1.0349	2.4590	1.1467	2.6956	1.2570	2.9295	1.3661	3.1611	1.4741	3.3909	1.5812	3.6196	1.6876		
2.8034	1.0204	3.1143	1.1335	3.4204	1.2449	3.7226	1.3549	4.0216	1.4638	4.3219	1.5731	4.6117	1.6786		
3.7630	1.0083	4.1896	1.1226	4.6091	1.2350	5.0225	1.3458								
0	1.9000	0	2.0000	0	2.1000	0	2.2000	0	2.3000	0	2.4000	0	2.5000		
.1662	1.8991	.1749	1.9991	.1837	2.0991	.1924	2.1992	.2012	2.2992	.2099	2.3992	.2187	2.4993		
.3344	1.8963	.3521	1.9965	.3647	2.0966	.3874	2.1967	.4050	2.2969	.4227	2.3970	.4403	2.4971		
.5069	1.8918	.5338	1.9921	.5607	2.0925	.5876	2.1928	.6145	2.2931	.6413	2.3934	.6682	2.4936		
.6863	1.8855	.7229	1.9862	.7595	2.0867	.7961	2.1873	.8327	2.2878	.8693	2.3883	.9058	2.4887		
.8757	1.8778	.9228	1.9788	.9698	2.0797	1.0168	2.1806	1.0638	2.2813	1.1108	2.3821	1.1578	2.4828		
1.0790	1.8688	1.1375	1.9702	1.1960	2.0715	1.2544	2.1727	1.3128	2.2738	1.3711	2.3748	1.4294	2.4758		
1.3015	1.8587	1.3728	1.9606	1.4441	2.0623	1.5152	2.1639	1.5863	2.2654	1.6572	2.3668	1.7281	2.4680		
1.5505	1.8478	1.6365	1.9502	1.7223	2.0525	1.8079	2.1545	1.8933	2.2564	1.9787	2.3581	2.0640	2.4597		
1.8365	1.8365	1.9395	1.9395	2.0422	2.0422	2.1447	2.1447	2.2469	2.2469	2.3490	2.3490	2.4510	2.4510		
2.1750	1.8250	2.2984	1.9286	2.4214	2.0318	2.5441	2.1348	2.6665	2.2375	2.7887	2.3400	2.9106	2.4423		
2.5885	1.8125	2.7390	1.9179	2.8872	2.0217	3.0349	2.1251	3.1822	2.2282	3.3292	2.3311	3.4758	2.4338		
3.1231	1.8031	3.3044	1.9078	3.4850	2.0121	3.6649	2.1159	3.8443	2.2195	4.0232	2.3228	4.2016	2.4258		
3.8458	1.7933	4.0714	1.8986	4.2960	2.0033	4.5197	2.1076	4.7426	2.2115	4.9648	2.3152				
4.4035	1.7848														
		0	2.6000	0	2.7000	0	2.8000	0	2.9000	0	3.0000				
		.2274	2.5993	.2362	2.6994	.2449	2.7994	.2537	2.8994	.2625	2.9994				
		.4580	2.5972	.4756	2.6973	.4933	2.7974	.5109	2.8975	.5286	2.9975				
		.6950	2.5938	.7219	2.6941	.7487	2.7942	.7756	2.8944	.8024	2.9946				
		.9424	2.5892	.9789	2.6895	1.0154	2.7899	1.0520	2.8902	1.0885	2.9905				
		1.2047	2.5834	1.2516	2.6840	1.2984	2.7845	1.3453	2.8850	1.3922	2.9855				
		1.4876	2.5766	1.5459	2.6775	1.6040	2.7782	1.6622	2.8790	1.7203	2.9796				
		1.7990	2.5692	1.8698	2.6702	1.9405	2.7713	2.0112	2.8722	2.0818	2.9731				
		2.1491	2.5612	2.2342	2.6626	2.3191	2.7638	2.4041	2.8651	2.4889	2.9662				
		2.5528	2.5528	2.6545	2.6545	2.7561	2.7561	2.8576	2.8576	2.9589	2.9564				
		3.0324	2.5445	3.1539	2.6465	3.2753	2.7483	3.3965	2.8501	3.5176	2.9517				
		3.6222	2.5363	3.7683	2.6386	3.9142	2.7408	4.0598	2.8428	4.2053	2.9446				
		4.3796	2.5286	4.5573	2.6312	4.7347	2.7336								

TABLE II.- TABULATED VALUES OF THE PARAMETERS NECESSARY TO REFRODUCE CHART II IN FIGURE 2(b) - Concluded

(b) Lines of Constant Velocity Ratio (k)

k	$\frac{z'}{d}$	$\frac{y'}{d}$	k	$\frac{z'}{d}$	$\frac{y'}{d}$	k	$\frac{z'}{d}$	$\frac{y'}{d}$	k	$\frac{z'}{d}$	$\frac{y'}{d}$	k	$\frac{z'}{d}$	$\frac{y'}{d}$
0.200	0.5075	0.0511	0.850	0.6117	0.3404	1.000	0.9186	0.8478	1.100	0.5891	1.0455	1.400	0.3506	0.4558
	.5176	.0501		.7044	.3793		1.0897	1.0308		.5547	1.1757		.3437	.4919
	.5279	.0469		.8060	.4006		1.2625	1.2120		.4856	1.3131		.3337	.5285
	.5385	.0409		.9165	.4000		1.4369	1.3912		.3527	1.4580		.3200	.5658
	.5492	.0301		1.0363	.3691		1.6105	1.5713		.2272	1.5333		.3017	.6038
				1.1653	.2865		1.7854	1.7500		.0158	1.5809		.2775	.6427
0.300	.5041	.0774		1.2334	.2032		1.9606	1.9285					.2451	.6823
	.5191	.0786					2.1360	2.1066	1.150	.4480	.3991		.2000	.7229
	.5450	.0741	0.900	.5169	.3048		2.3117	2.2845		.4797	.5094		.1284	.7643
	.5721	.0578		.6355	.3983		2.4875	2.4622		.5004	.6242		.0083	.7905
	.5889	.0358		.8675	.4975		2.6634	2.6399		.5059	.7444			
				1.0847	.5134		2.8395	2.8174		.4899	.8718	1.500	.3297	.3825
0.400	.5140	.1067		1.2042	.4898					.4420	1.0101		.3286	.3900
	.5391	.1091		1.3313	.4332	1.025	.5725	.4846		.3373	1.1517		.3246	.4127
	.5654	.1048		1.4661	.3172		.7155	.6987		.2375	1.2273		.3152	.4507
	.5928	.0930		1.5364	.2051		.8486	.9179					.3020	.4894
	.6213	.0681					.9650	1.1484	1.200	.4085	.3298		.2837	.5287
	.6390	.0370	0.925	.5111	.3143		.9834	1.3941		.4165	.3592		.2590	.5688
				.5850	.3845		1.1192	1.6576		.4307	.4178		.2250	.6098
0.500	.5073	.1354		.7498	.4978		1.1386	1.9407		.4418	.4768		.1756	.6518
	.5314	.1419		.9375	.5755		1.1000	2.2450		.4493	.5368		.0857	.6947
	.5566	.1443		1.1486	.6089		.9739	2.5718		.4520	.5986		.0106	.7069
	.5829	.1425		1.3851	.5759		.6796	2.9220		.4498	.6616			
	.6102	.1356		1.5129	.5209		.4384	3.0689		.4406	.7270	1.600	.3073	.4008
	.6385	.1220		1.6472	.4204					.4229	.7945		.2950	.4161
	.6679	.0981		1.7882	.2048	1.050	.5580	.5012		.3942	.8644		.2860	.4403
	.6983	.0495					.6782	.7349		.3500	.9368		.2665	.4812
			0.950	.5051	.3239		.7704	.9844		.2816	1.0117		.2394	.5228
0.600	.4990	.1634		.6121	.4335		.8178	1.2576		.1527	1.0894		.2008	.5654
	.5219	.1738		.8124	.5831		.7952	1.5589		.0007	1.1180		.1406	.6090
	.5705	.1859		1.0401	.6934		.7292	1.7545				0		.6455
	.6229	.1858		1.2966	.7543		.6500	1.8915	1.300	.3819	.3380			
	.6791	.1698		1.5837	.7446		.5235	2.0337		.3846	.3574	1.700	.2590	.4335
	.7391	.1275		1.9033	.6144		.2853	2.1815		.3896	.3881		.2544	.4421
	.7705	.0833		2.0405	.4963					.3904	.4222		.2382	.4679
				2.1828	.2748	1.075	.4715	.3711		.3913	.4549		.2020	.5116
0.700	.5103	.2052					.5427	.5177		.3906	.4880		.1457	.5563
	.5555	.2267	0.975	.4989	.3333		.6045	.6668		.3881	.5215		.0869	.5836
	.6040	.2403		.5995	.4507		.6379	.7702		.3835	.5555		.0108	.5974
	.6557	.2451		.7822	.6230		.6781	.9901		.3766	.5905			
	.7107	.2396		.9820	.7735		.6805	1.1077		.3670	.6253	1.800	.2106	.4590
	.7690	.2205		1.1990	.9014		.6322	1.3603		.3542	.6611		.2025	.4680
	.8307	.1804		1.4342	1.0029		.5680	1.4958		.3375	.6977		.1842	.4681
	.8956	.0888		1.6890	1.0712		.2210	1.7864		.3160	.7350		.1619	.5047
				1.9645	1.0970					.2884	.7730		.1336	.5233
0.800	.5378	.2662		2.2619	1.0648	1.100	.4294	.3046		.2521	.8118		.0937	.5420
	.6277	.3100		2.5822	.9460		.4411	.3286		.2021	.8514			
	.7280	.3318		2.9261	.6620		.4638	.3807		.1216	.8918	1.900	.1424	.4845
	.8389	.3261		3.0704	.4274		.5071	.4827		.0210	.9123		.1264	.4941
	.9605	.2784					.5445	.5861					.1073	.5037
	1.0400	.2102	1.000	.4925	.3428		.5742	.6931	1.400	.3572	.3640		.0829	.5134
				.5863	.4677		.5937	.8047		.3569	.3851		.0451	.5231
0.850	.5276	.2859		.7500	.6615		.6000	.9227		.3520	.4226			

NACA

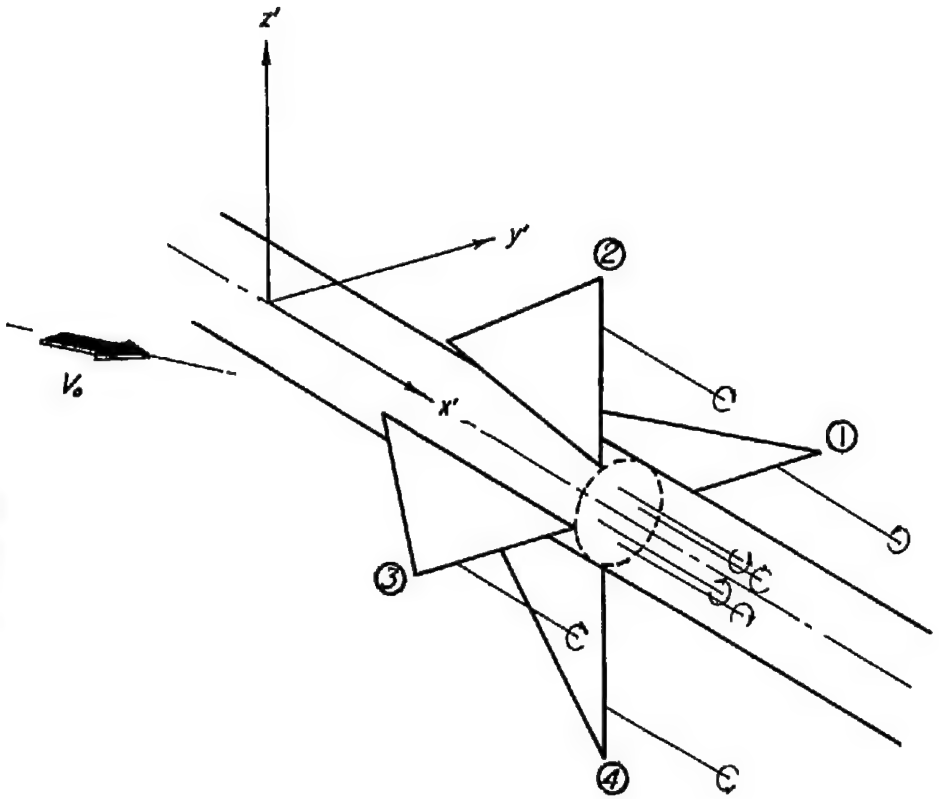

(a) Three-dimensional view showing wing and body and vortex filament arrangement.

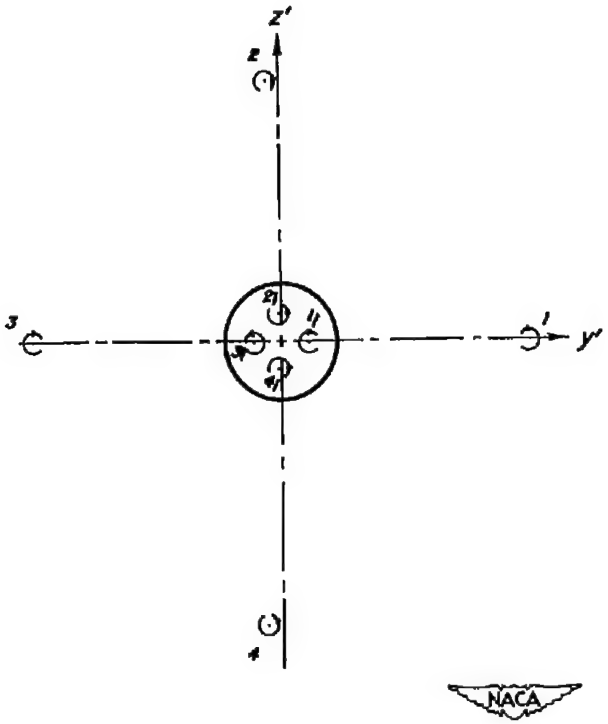

(b) Vortex positions in the plane of the wing trailing edge.

Figure 1.- Simplified model of a lifting cruciform-wing and body combination.

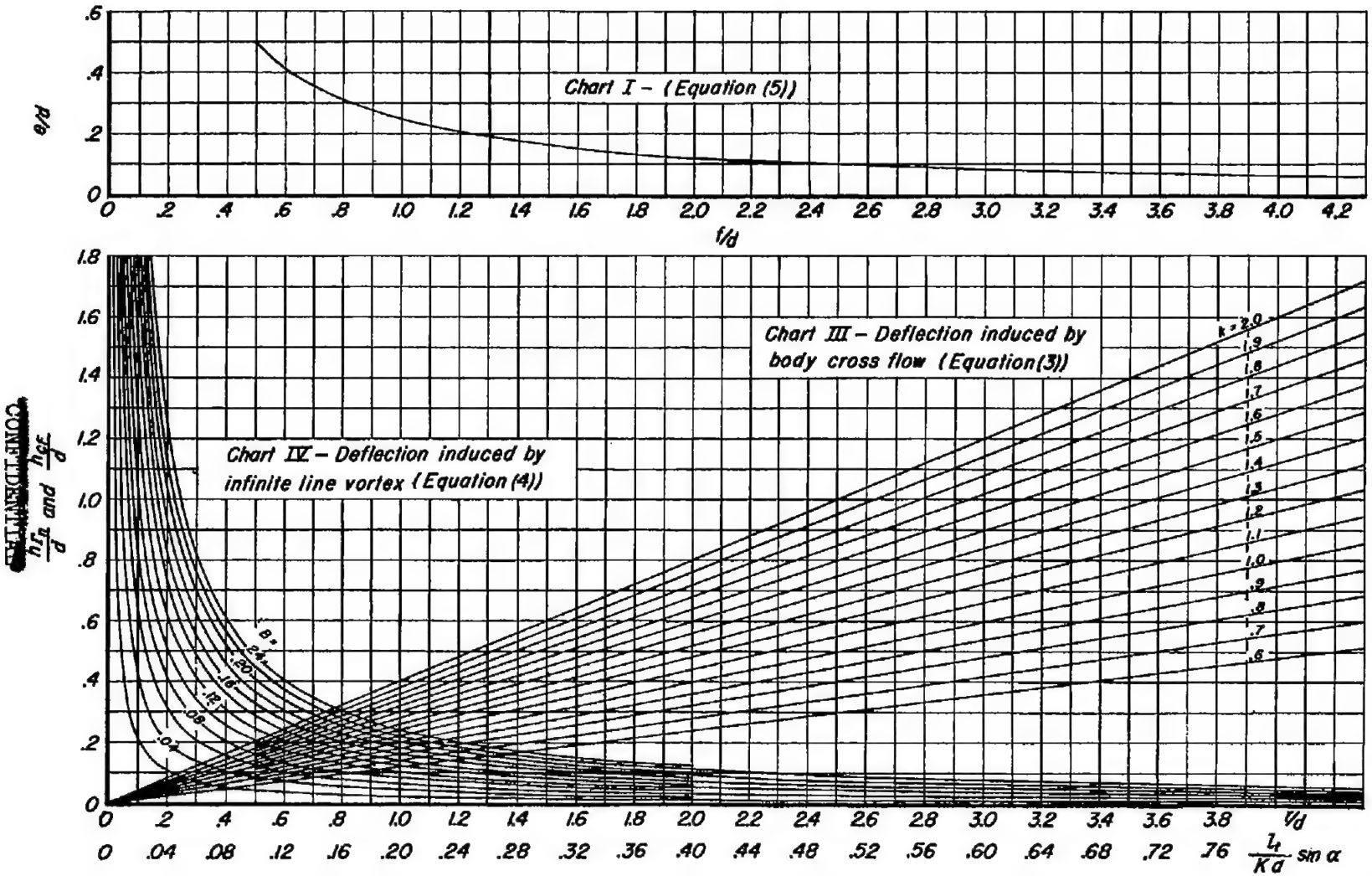

(a) Graphs of the aerodynamic and geometric parameters given in equations (3), (4), and (5).

Figure 2.- Charts for determining vortex motions graphically.

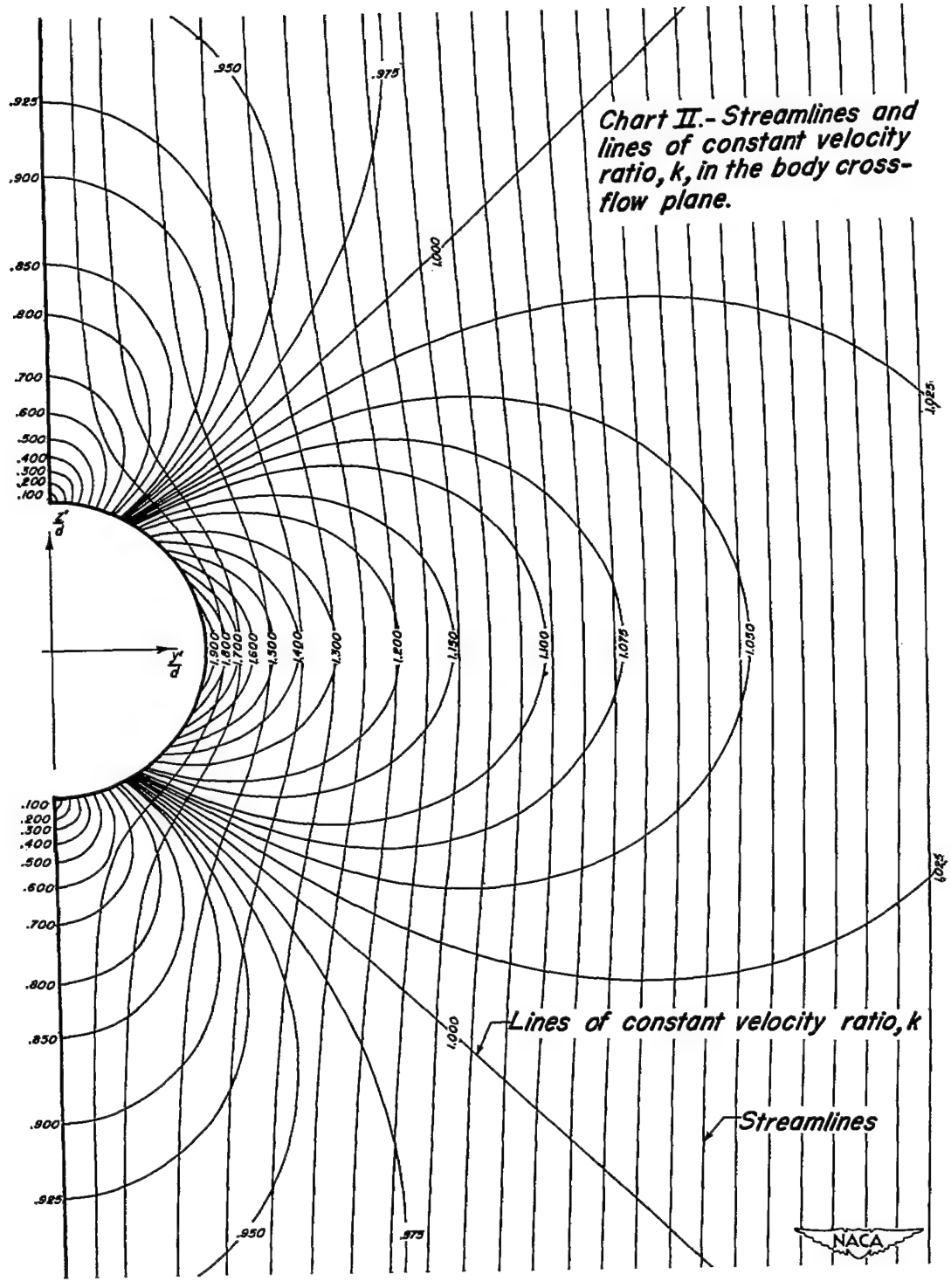

(b) Two-dimensional flow about an infinite circular cylinder.

Figure 2.- Concluded.

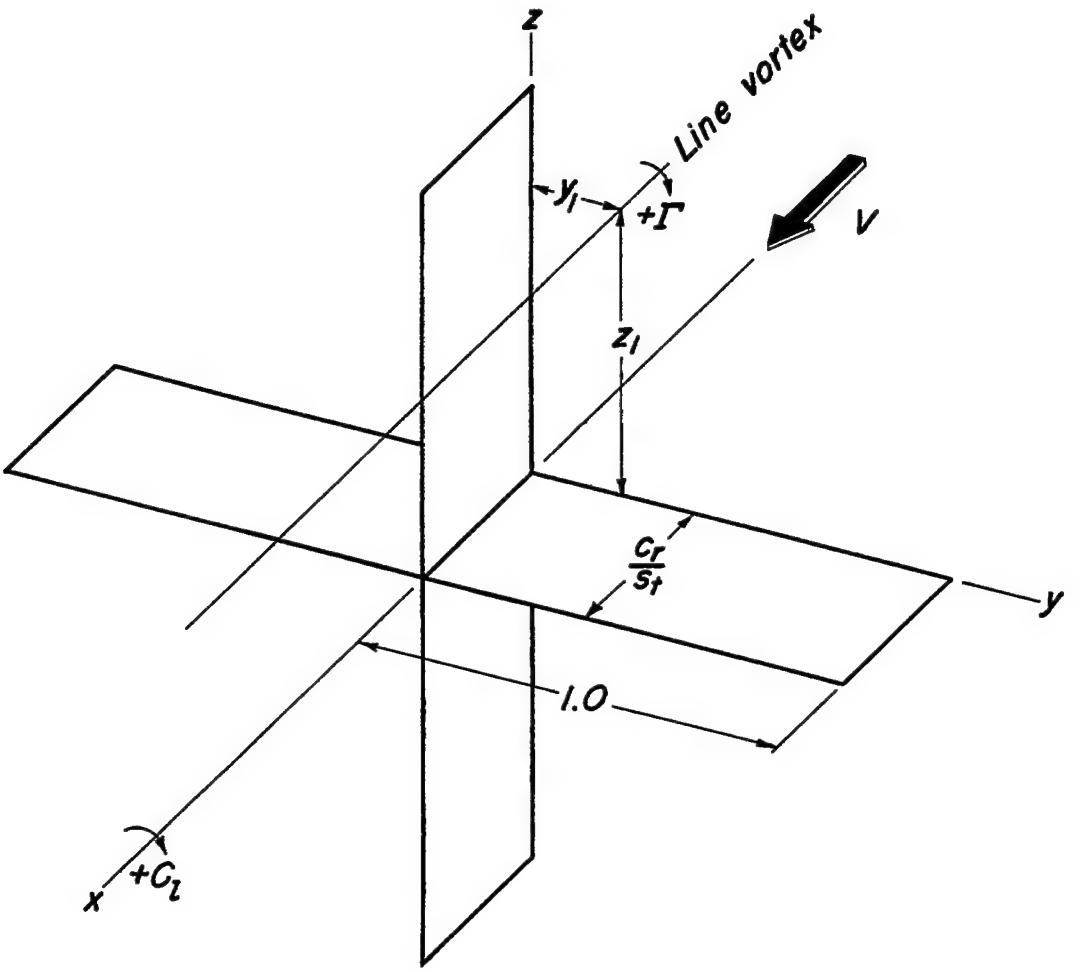

All dimensions in terms of the trailing wing semispan, s_t

NACA

Figure 3.- Geometric relations for obtaining the spanwise variation of the downwash angle on a cruciform wing of rectangular plan form.

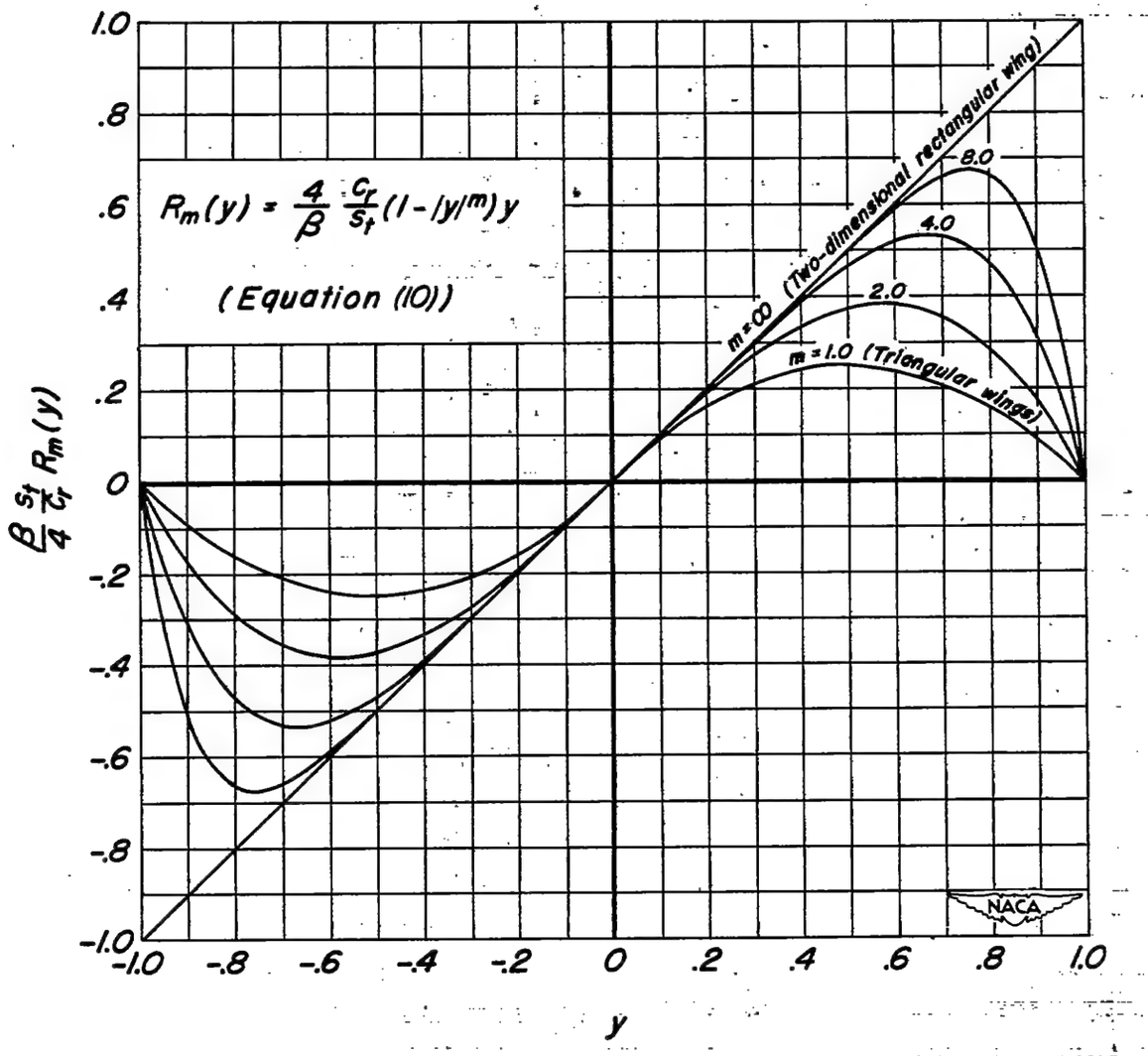

Figure 4. - Roll influence functions for various values of m in equation (10).

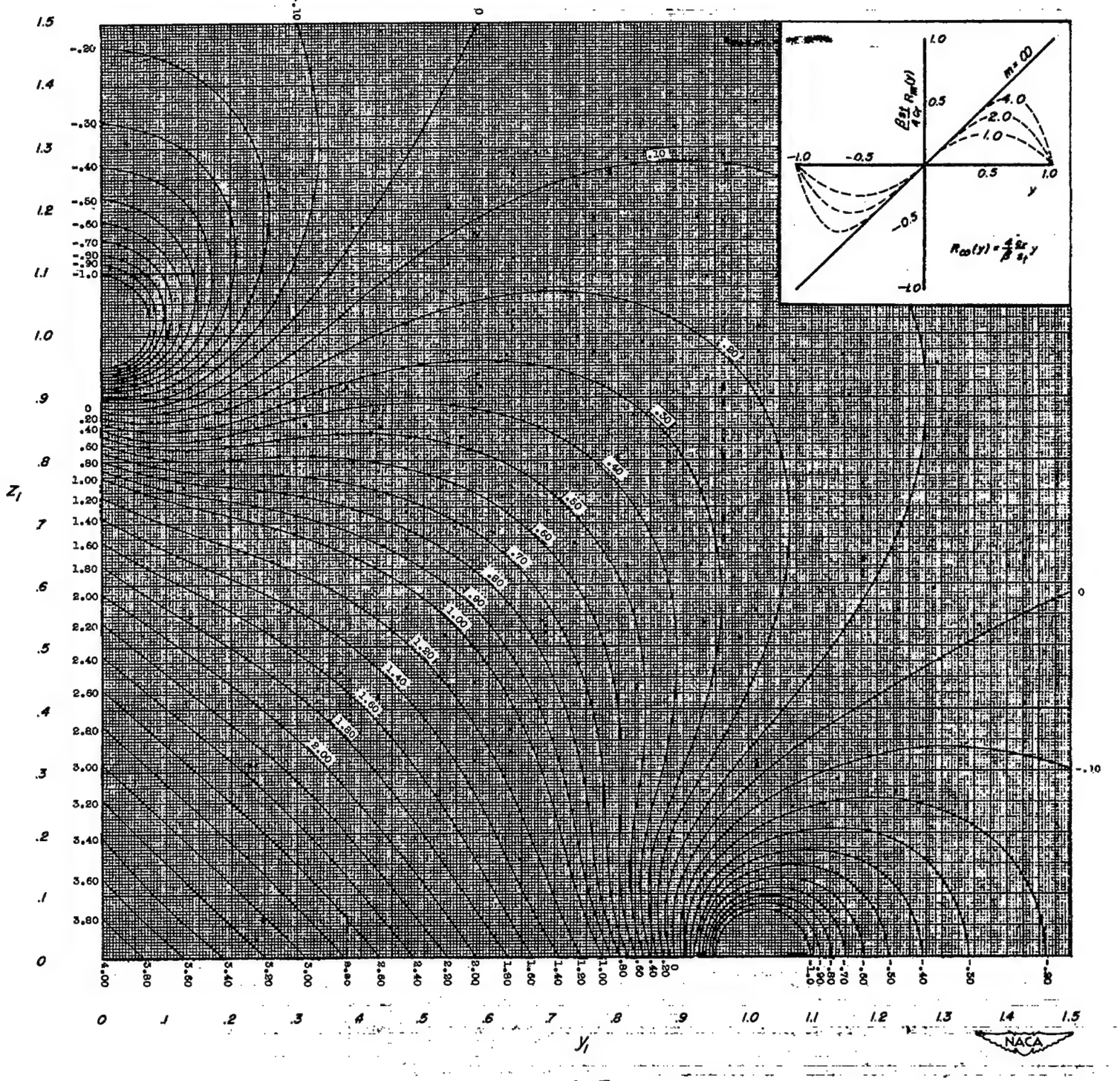

(a) F_∞

Figure 5.- Charts for determining values of the rolling-moment parameter, F_m, as a function of the vortex coordinates (y_1, z_1).

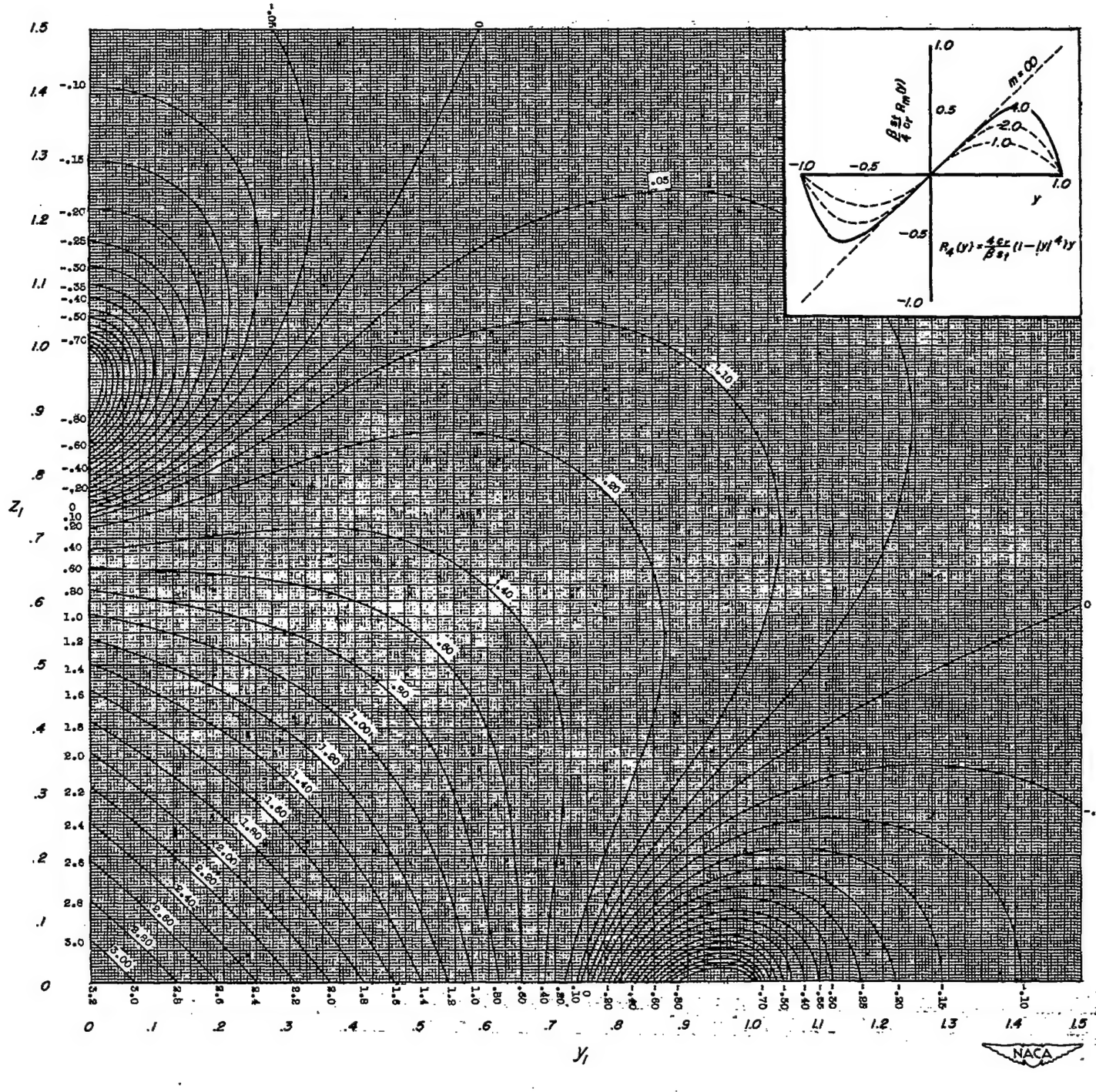

(b) F_4

Figure 5.- Continued.

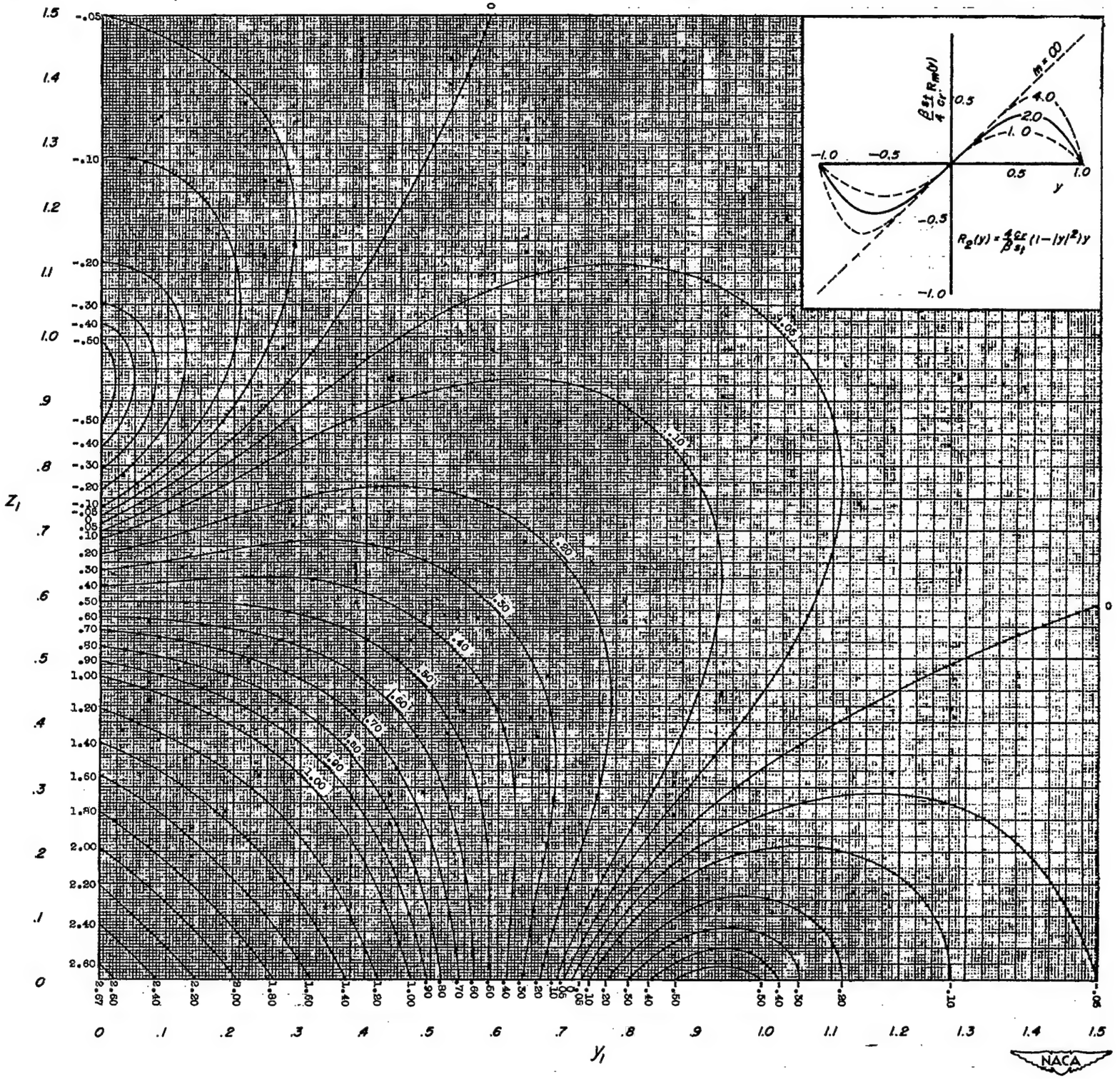

(c) F_2

Figure 5.- Continued.

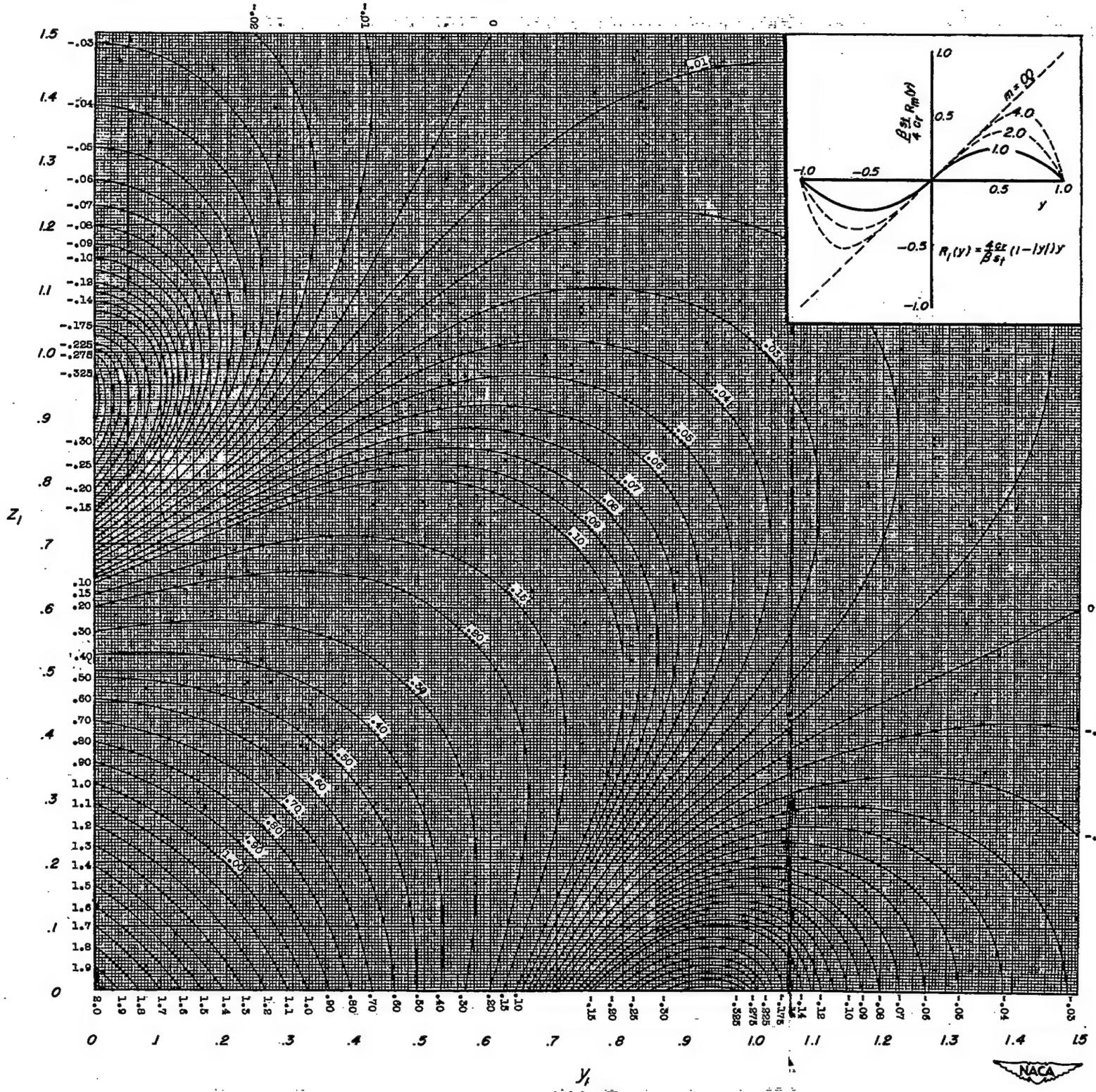

(d) F_1

Figure 5.- Concluded.

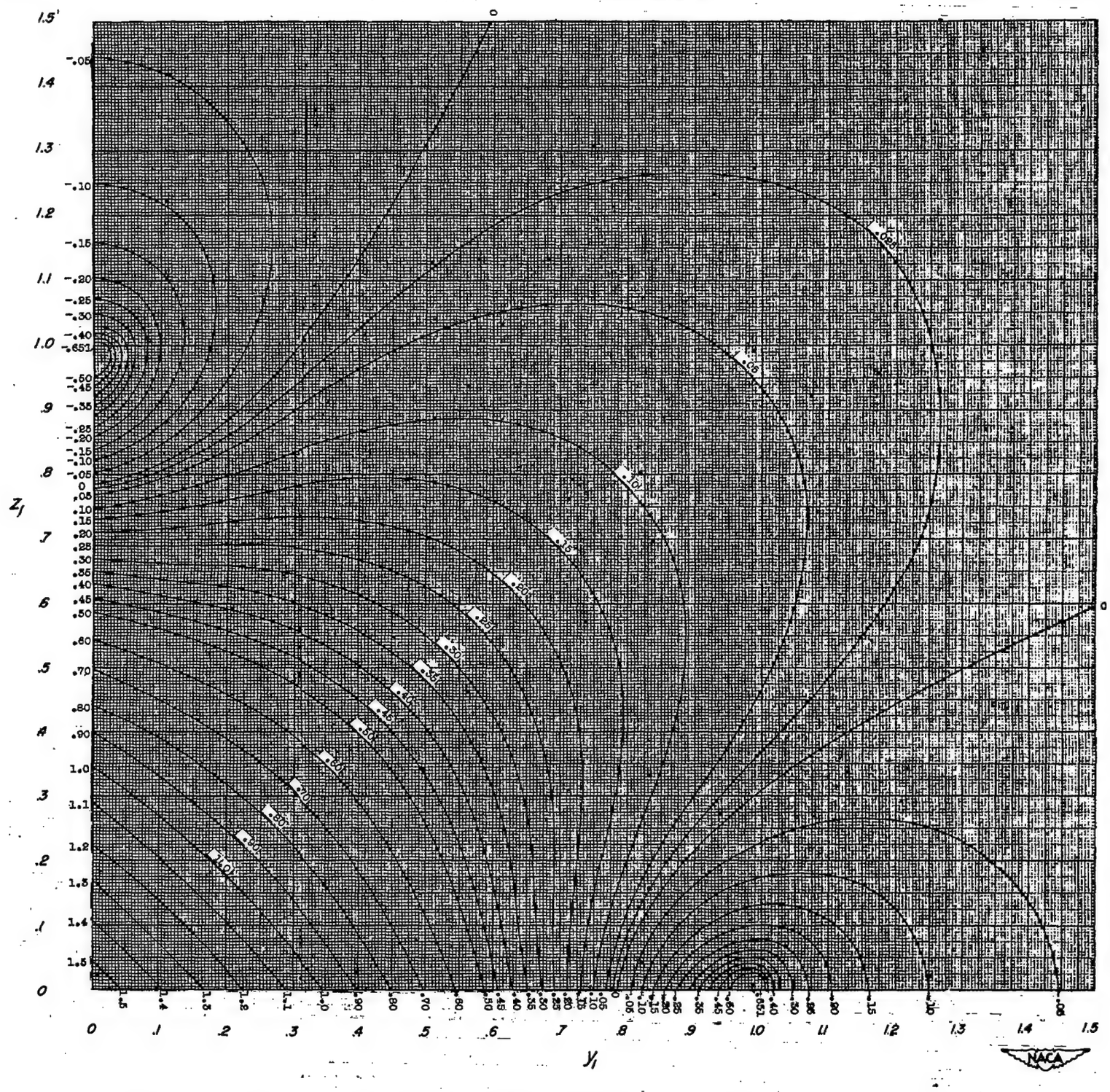

Figure 6.- Chart for determining values of the rolling-moment parameter, F_A, as a function of the vortex coordinates (y_1, z_1).

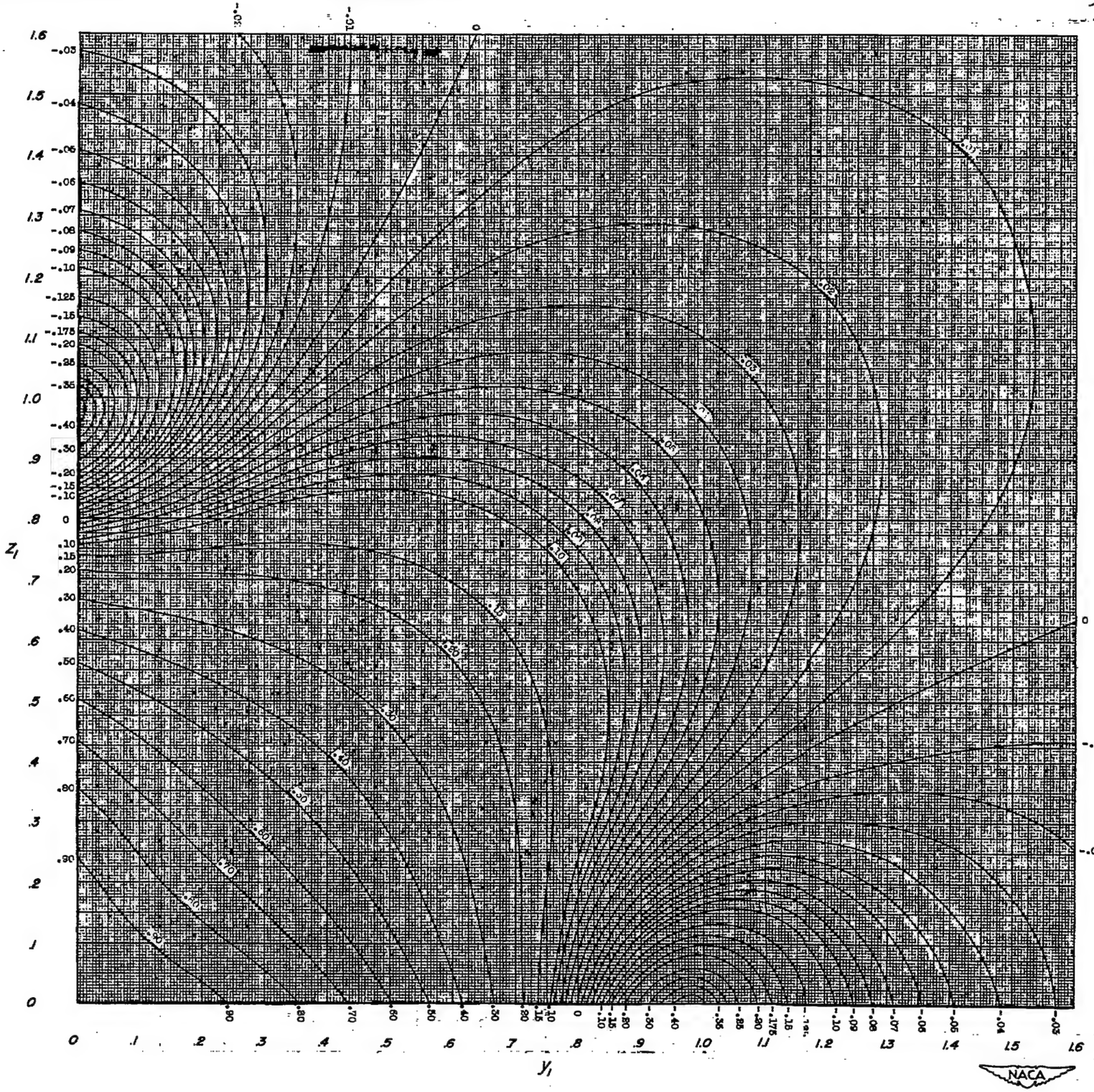

Figure 7.- Chart for determining values of the rolling-moment parameter, F_B, as a function of the vortex coordinates (y_1, z_1).

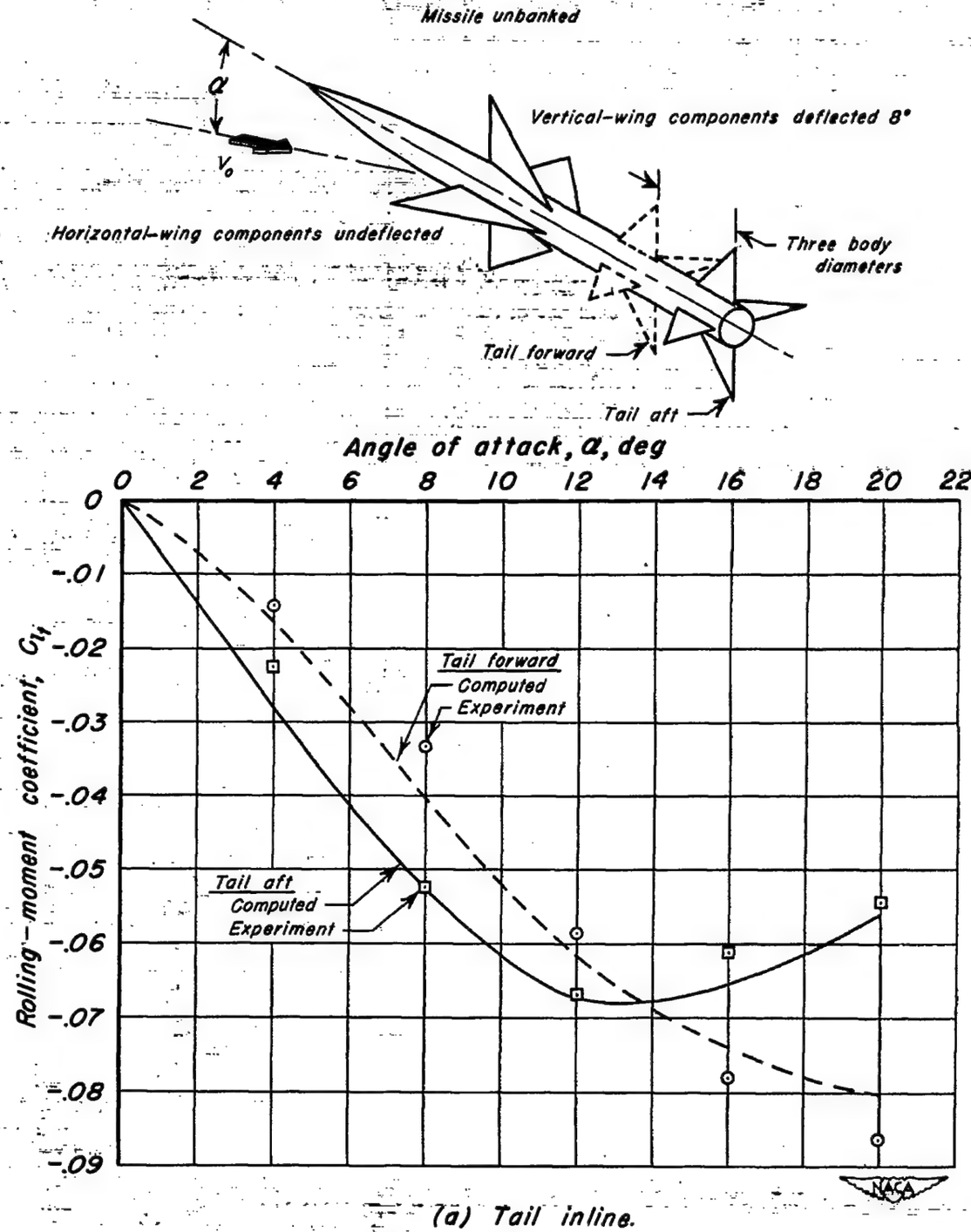

(a) Tail inline.

Figure 8.- Calculated and experimental tail rolling moments at 1.4 Mach number for Missile A.

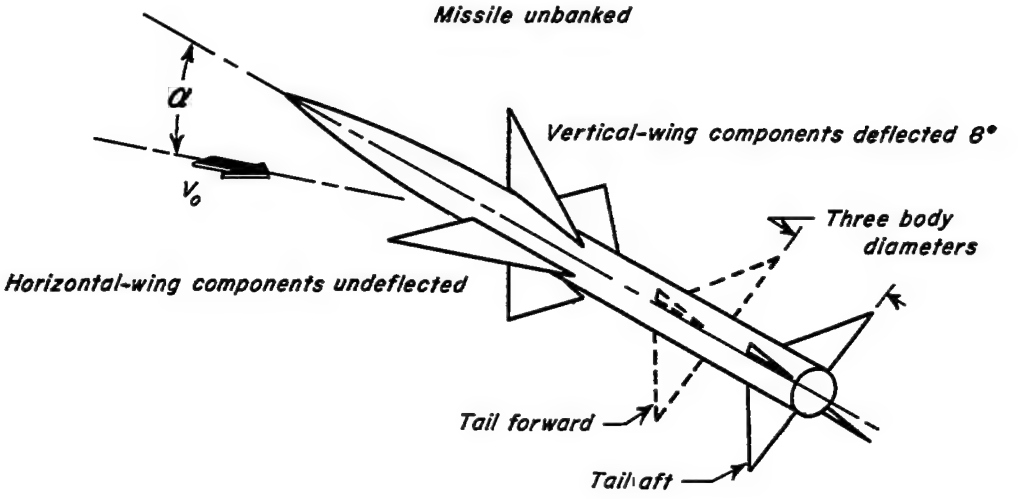

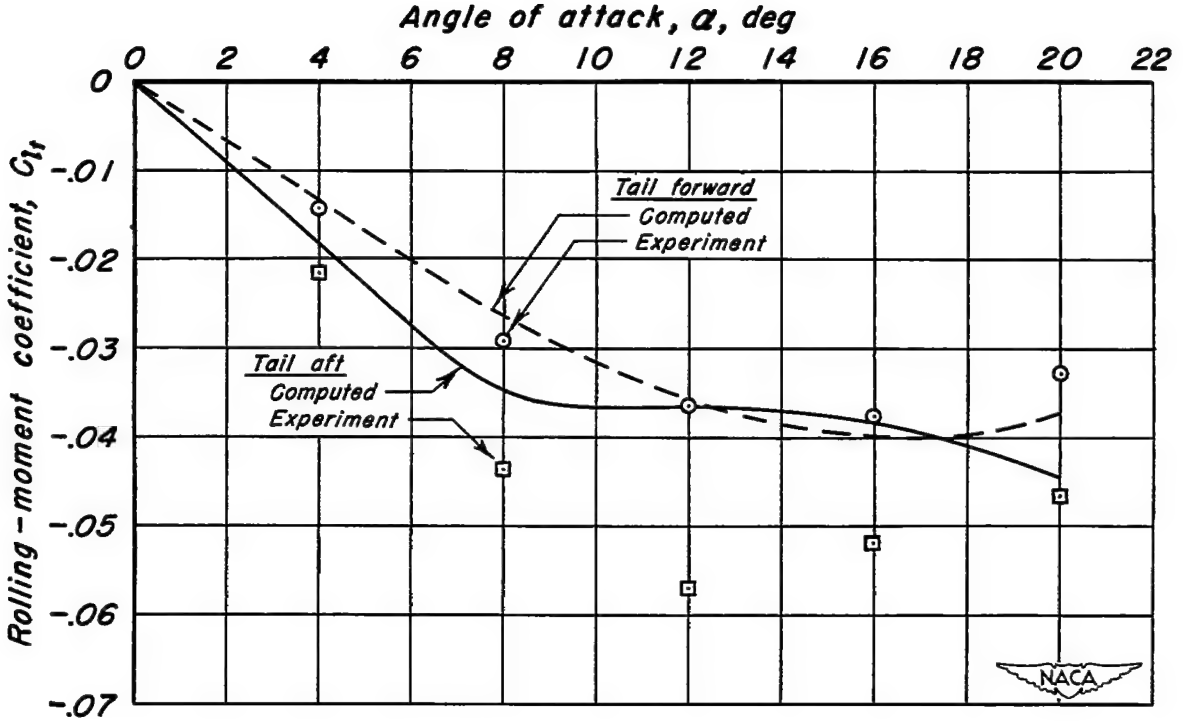

(b) Tail interdigitated.

Figure 8.- Concluded.

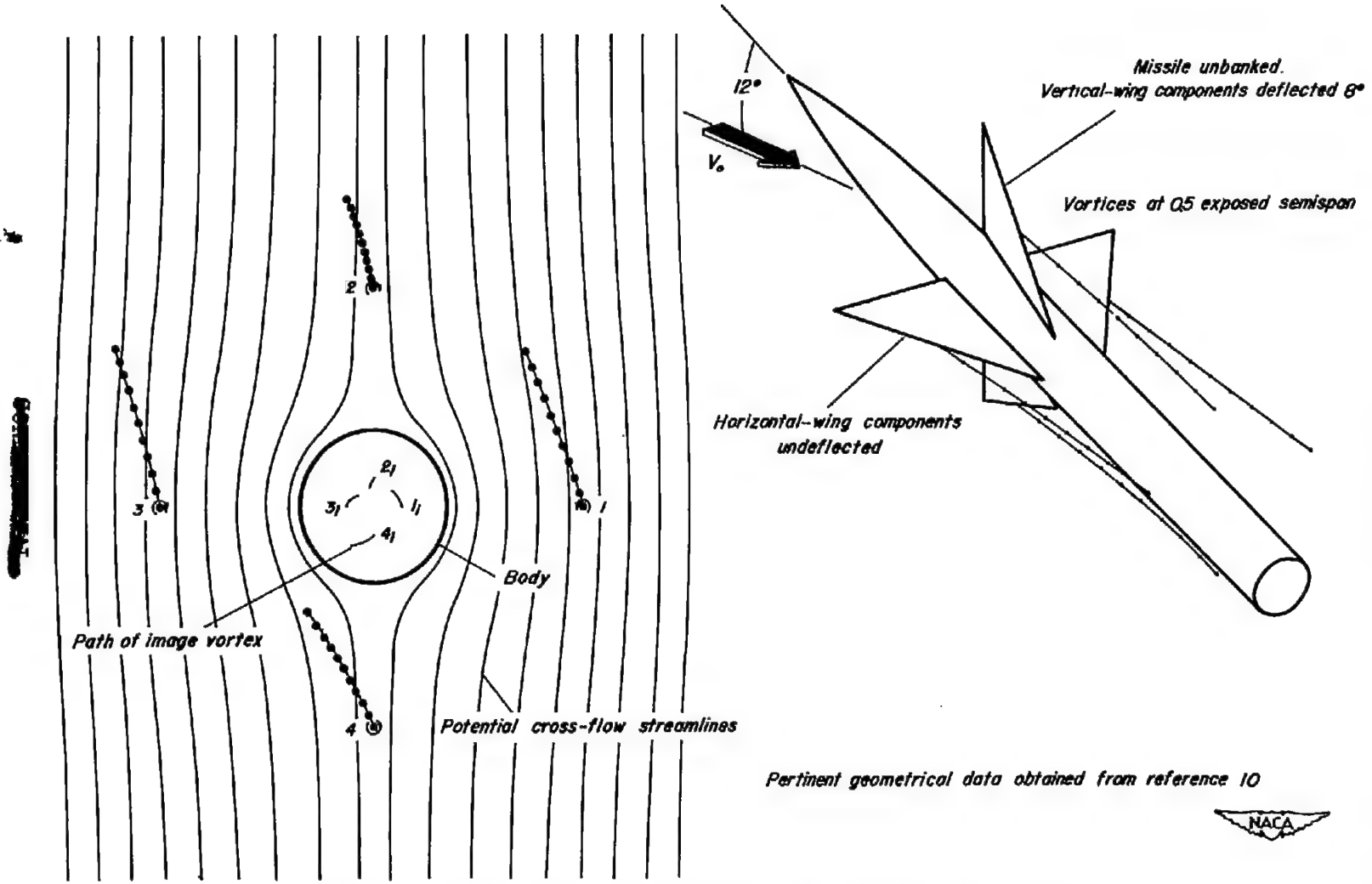

Figure 9. – Vortex paths downstream of the control fins of missile A at 12° angle of attack.

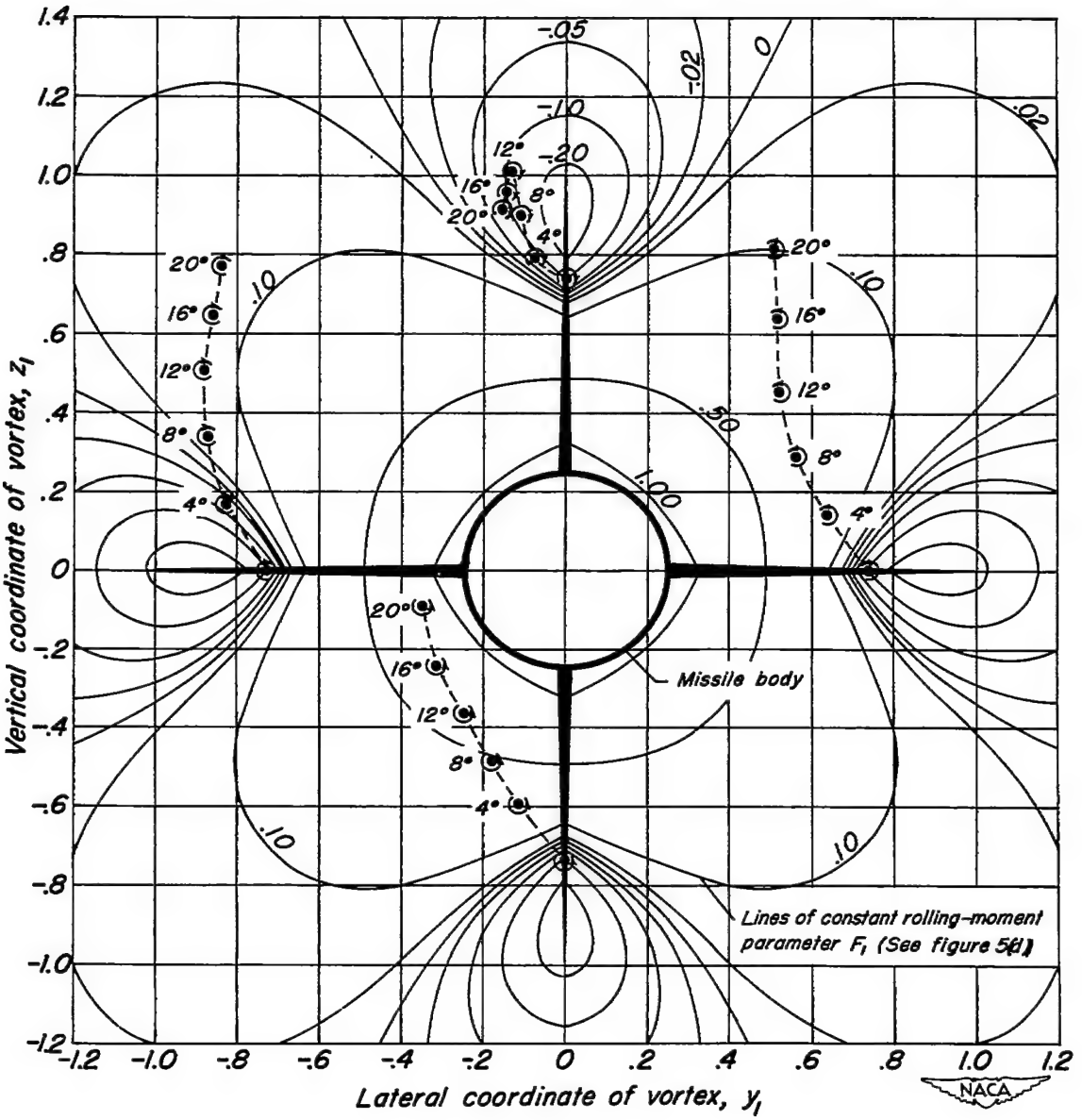

Figure 10.—Relationship between the position of the vortex cores at various angles of attack and lines of constant rolling-moment parameter, F_1, in the cross-flow plane at the center of pressure of the trailing wing of missile A at 1.4 Mach number.

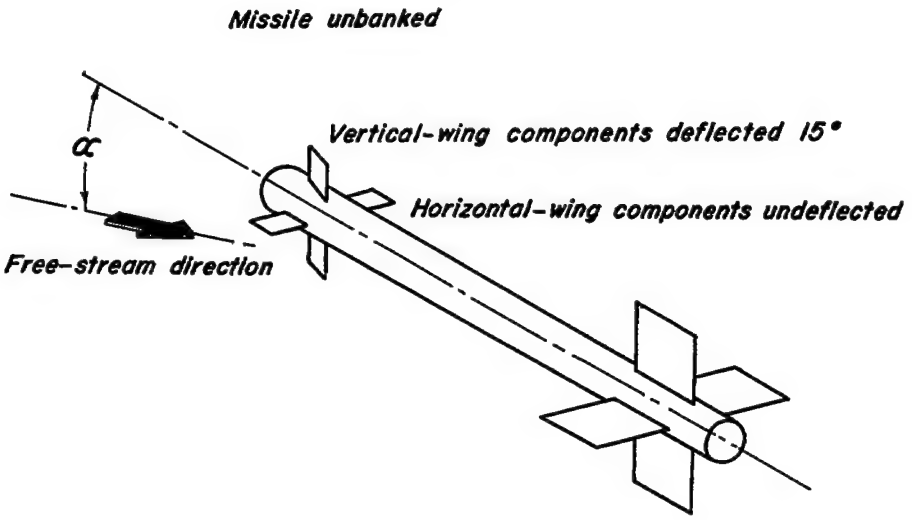

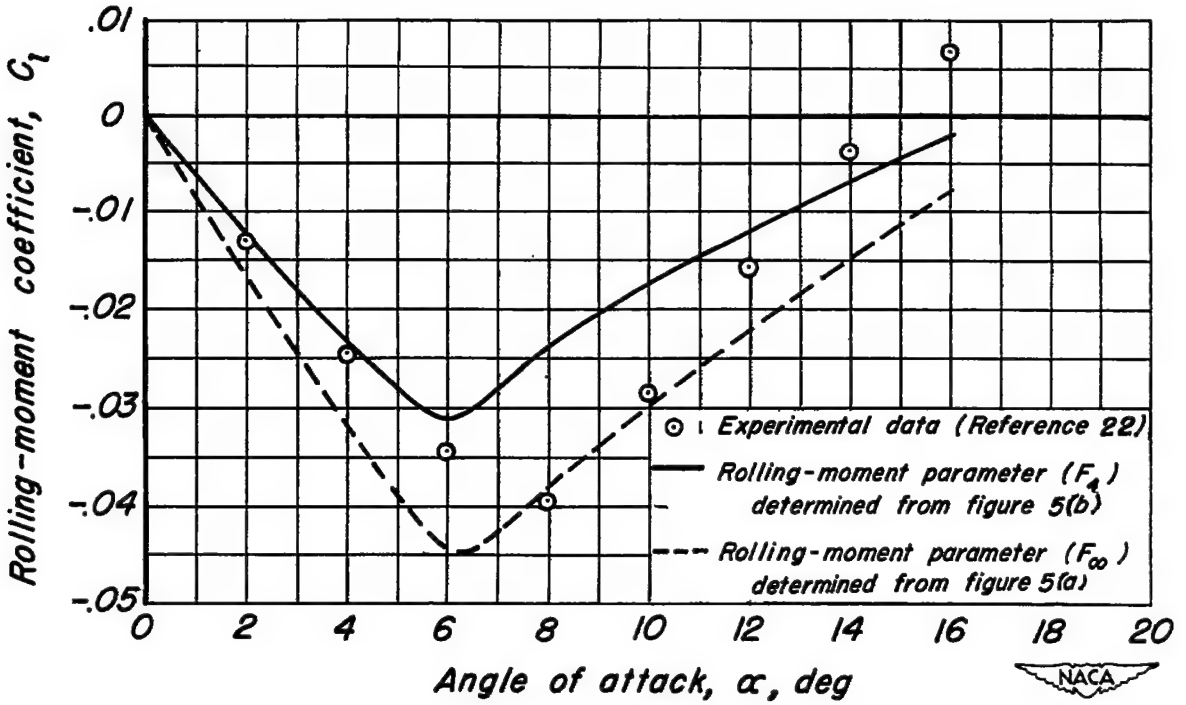

Figure 11.- Calculated and experimental tail rolling moments for missile B at 1.7 Mach number.

[redacted]

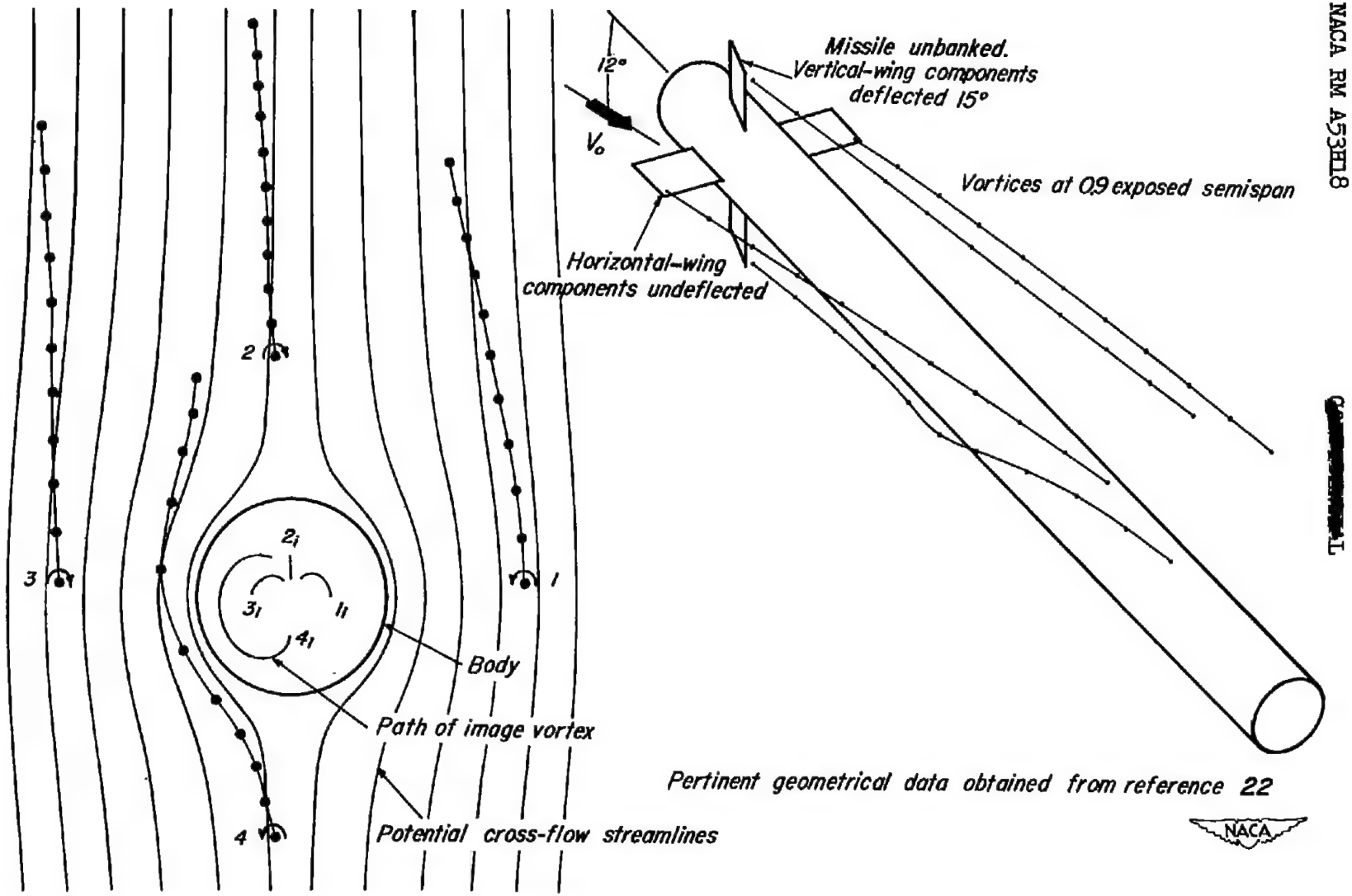

Figure 12.–Vortex paths downstream of the control fins of missile B at 12° angle of attack.

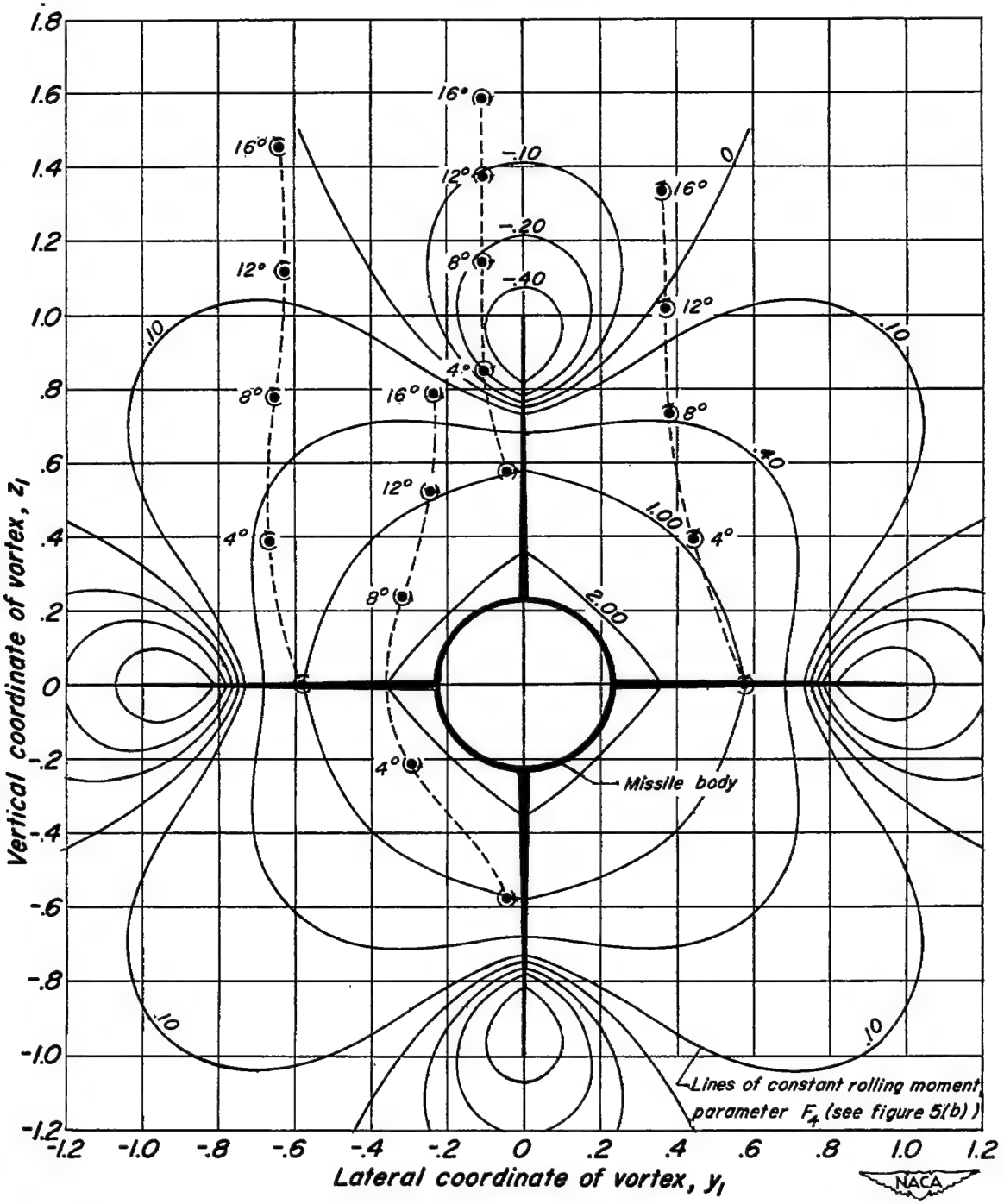

Figure 13.—Relationship between the position of the vortex cores at various angles of attack and lines of constant rolling-moment parameter, F_4, in the cross-flow plane at the center of pressure of the trailing wing of missile B at 1.7 Mach number.

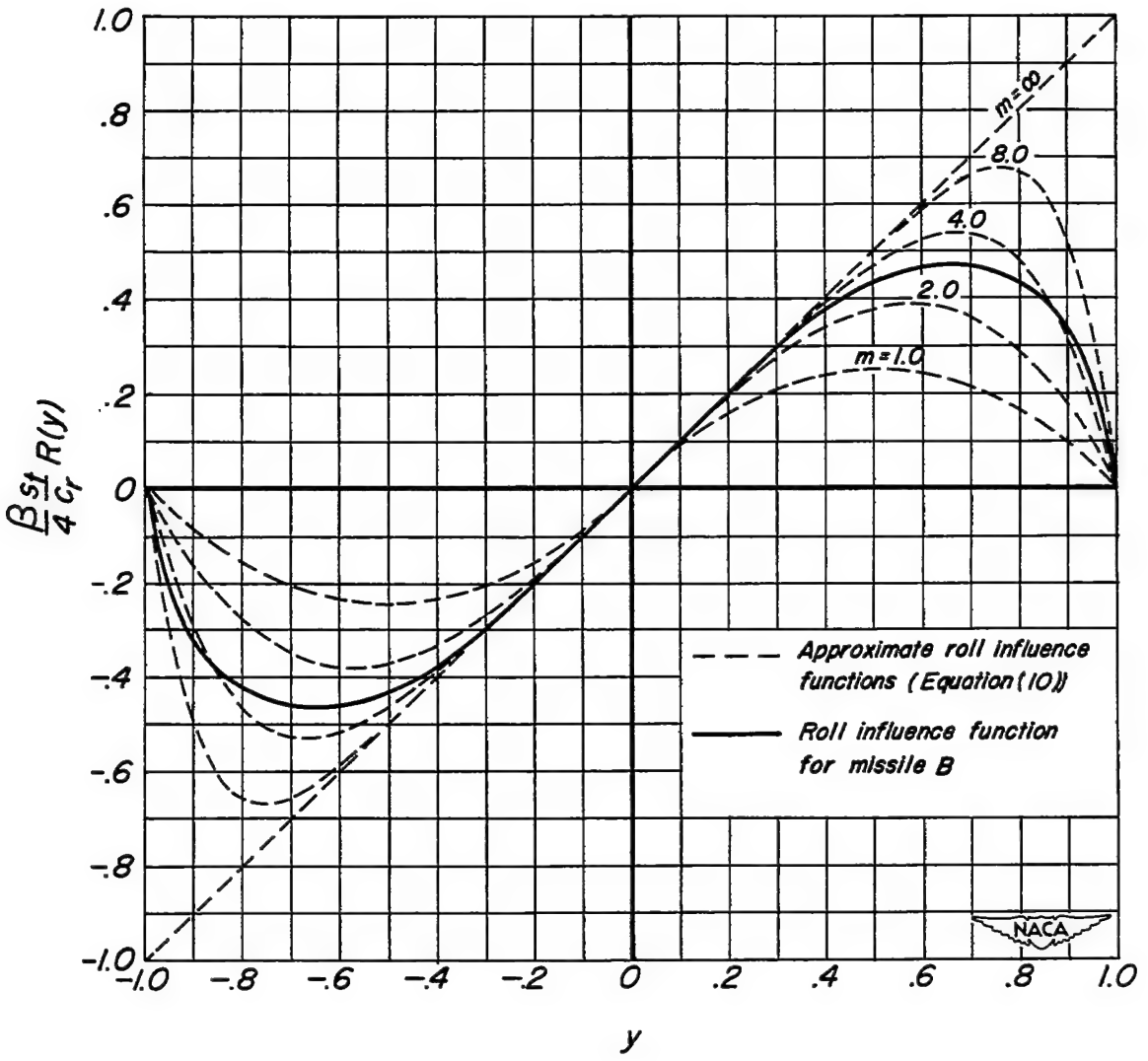

Figure 14. - Roll-influence function for missile B compared with approximate roll-influence functions shown in figure 4.

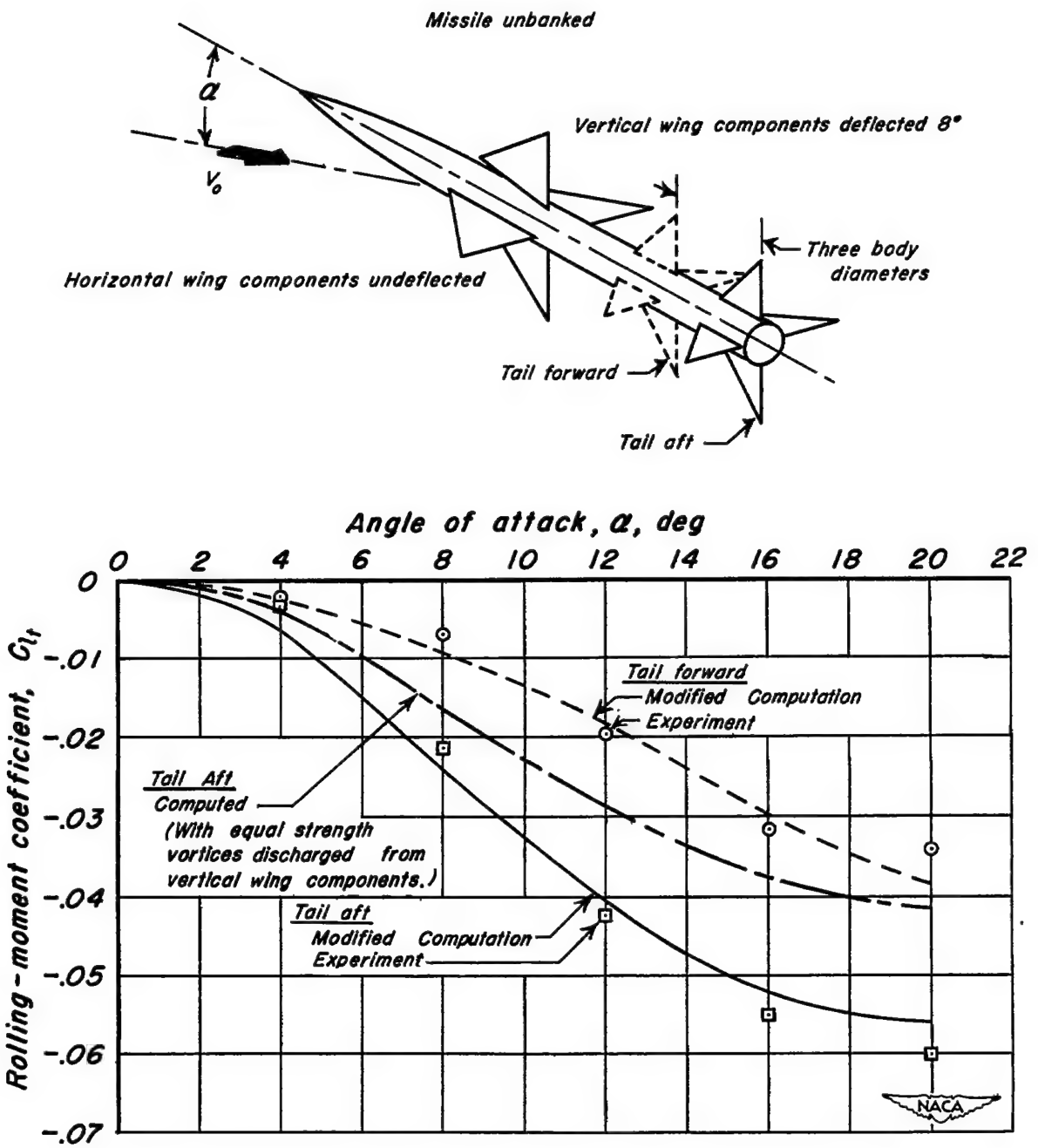

(a) Tail inline.

Figure 15.- Calculated and experimental tail rolling moments for missile C at 1.4 Mach number.

[redacted]

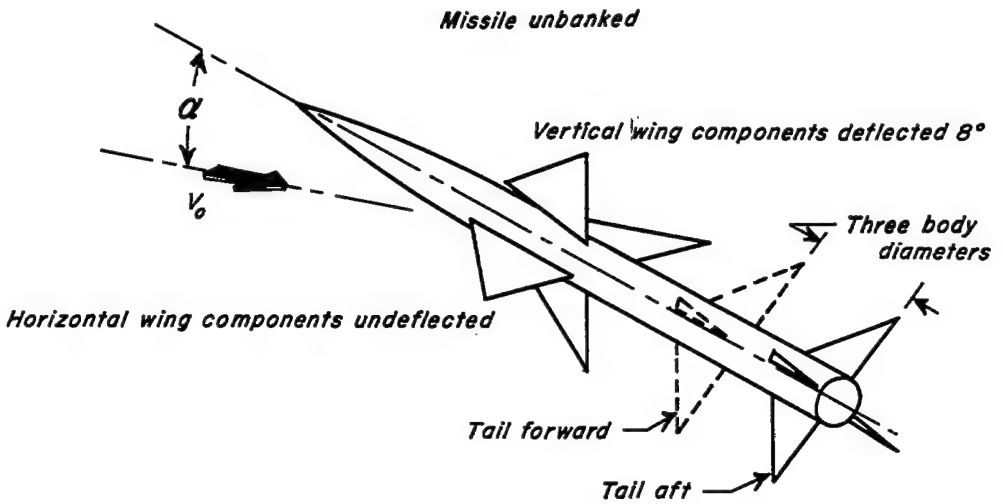

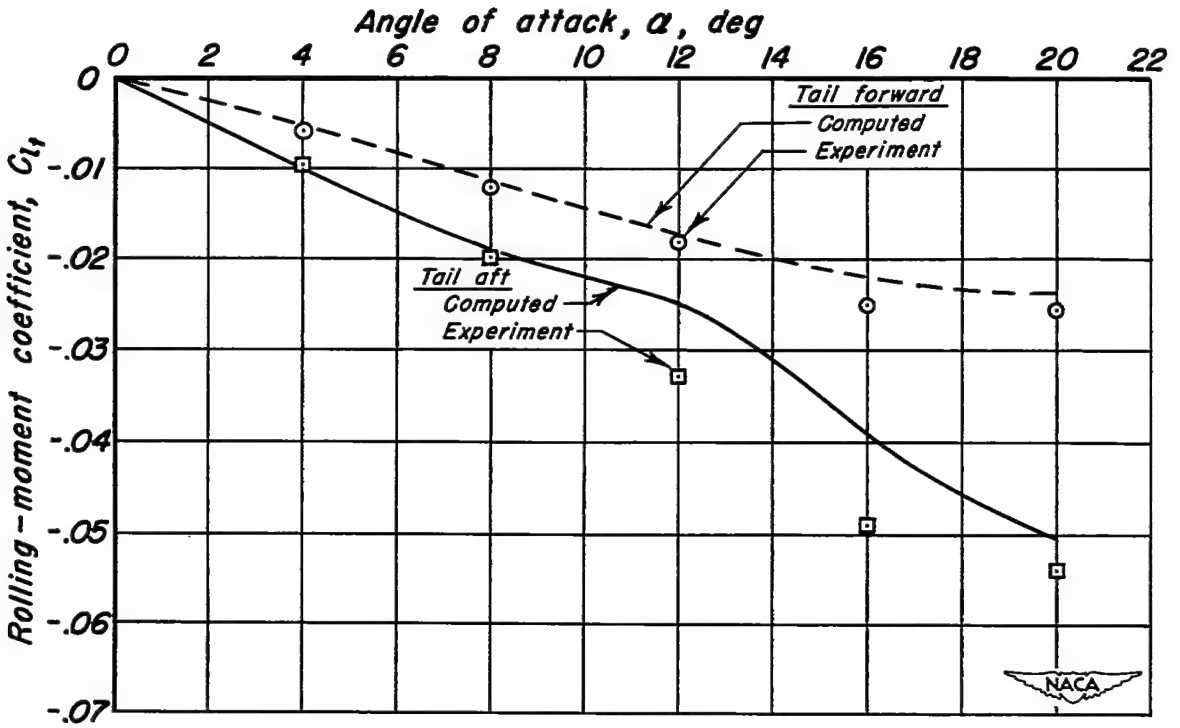

(b) Tail interdigitated.

Figure 15.- Concluded.

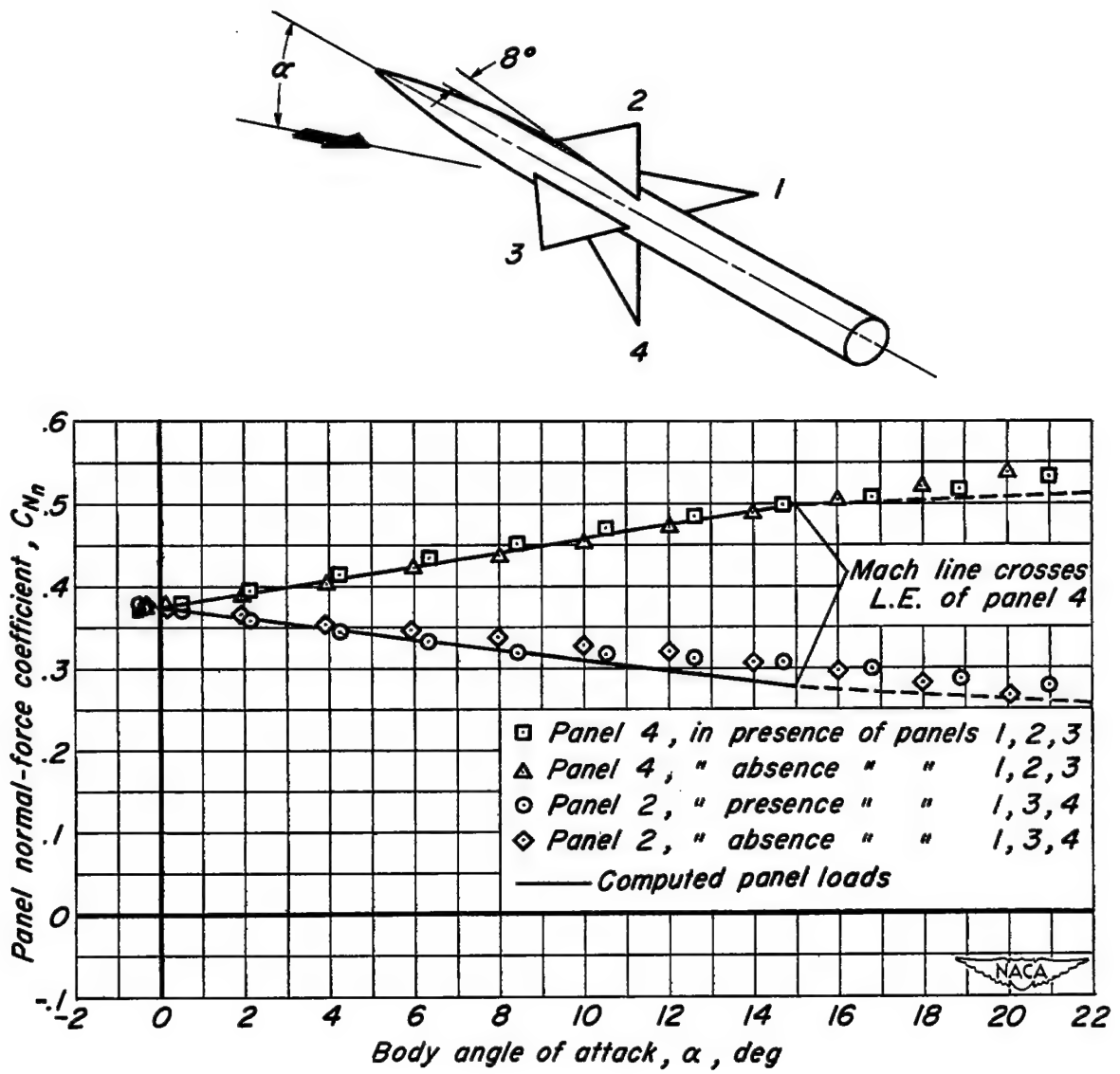

(a) Configuration unbanked with the vertical wing components deflected 8° with respect to the body center line.

Figure 16.- Individual panel normal-force coefficients for missile C at 1.4 Mach number.

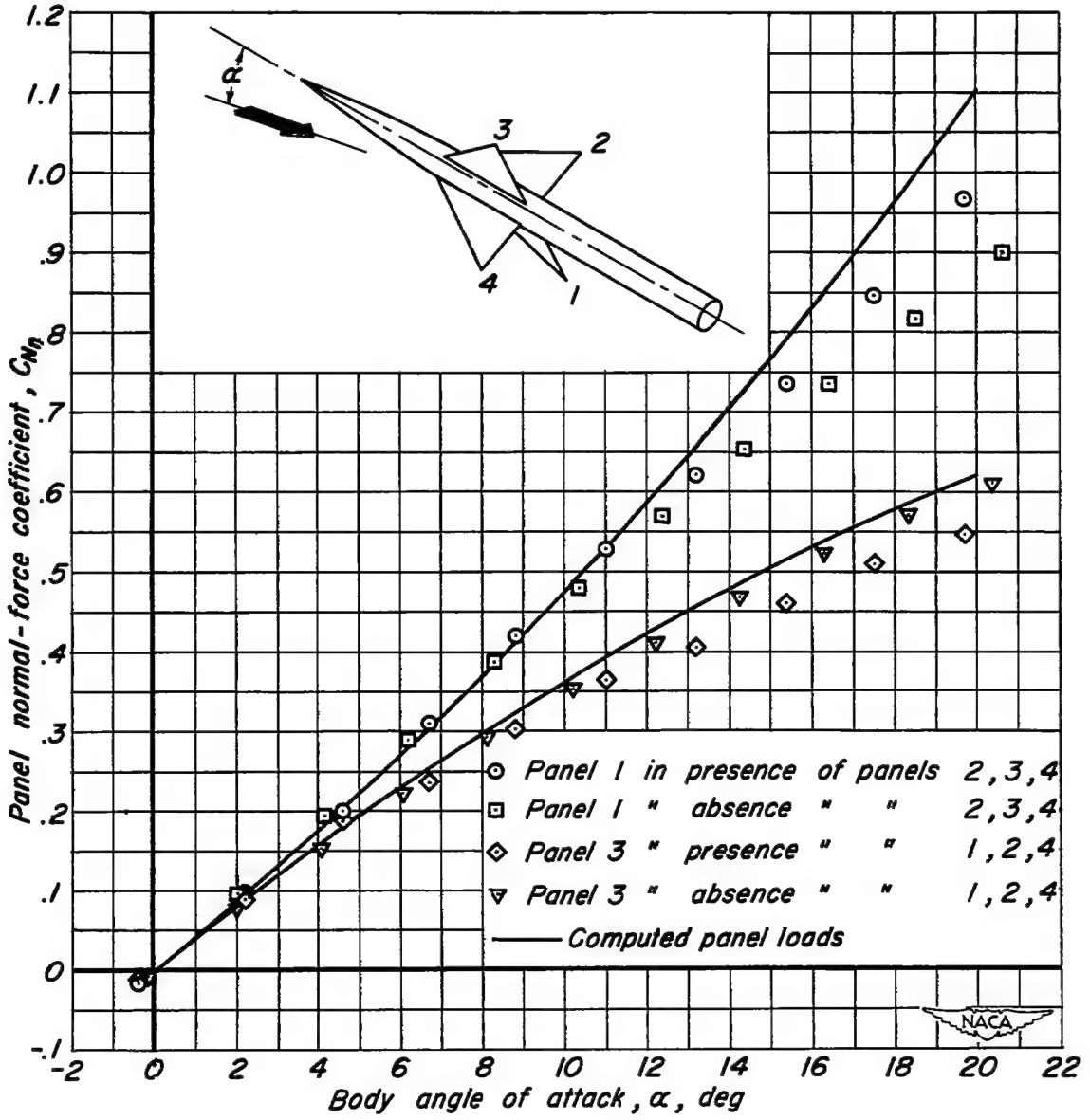

(b) Configuration banked 45° with the panels undeflected with respect to the body centerline.

Figure 16.- Concluded.

[redacted]

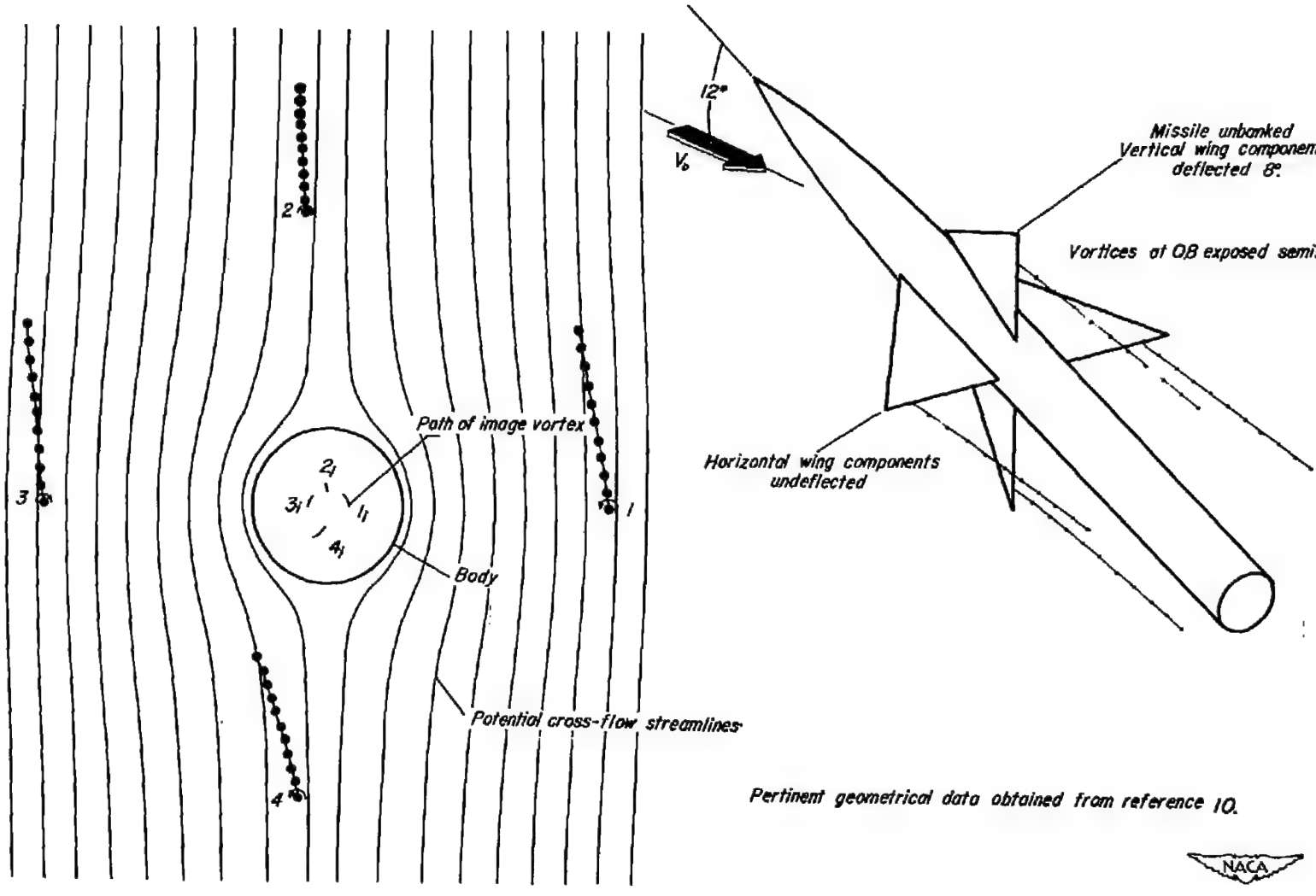

Figure 17. – Vortex paths downstream of the control fins of missile C at 12° angle of attack.

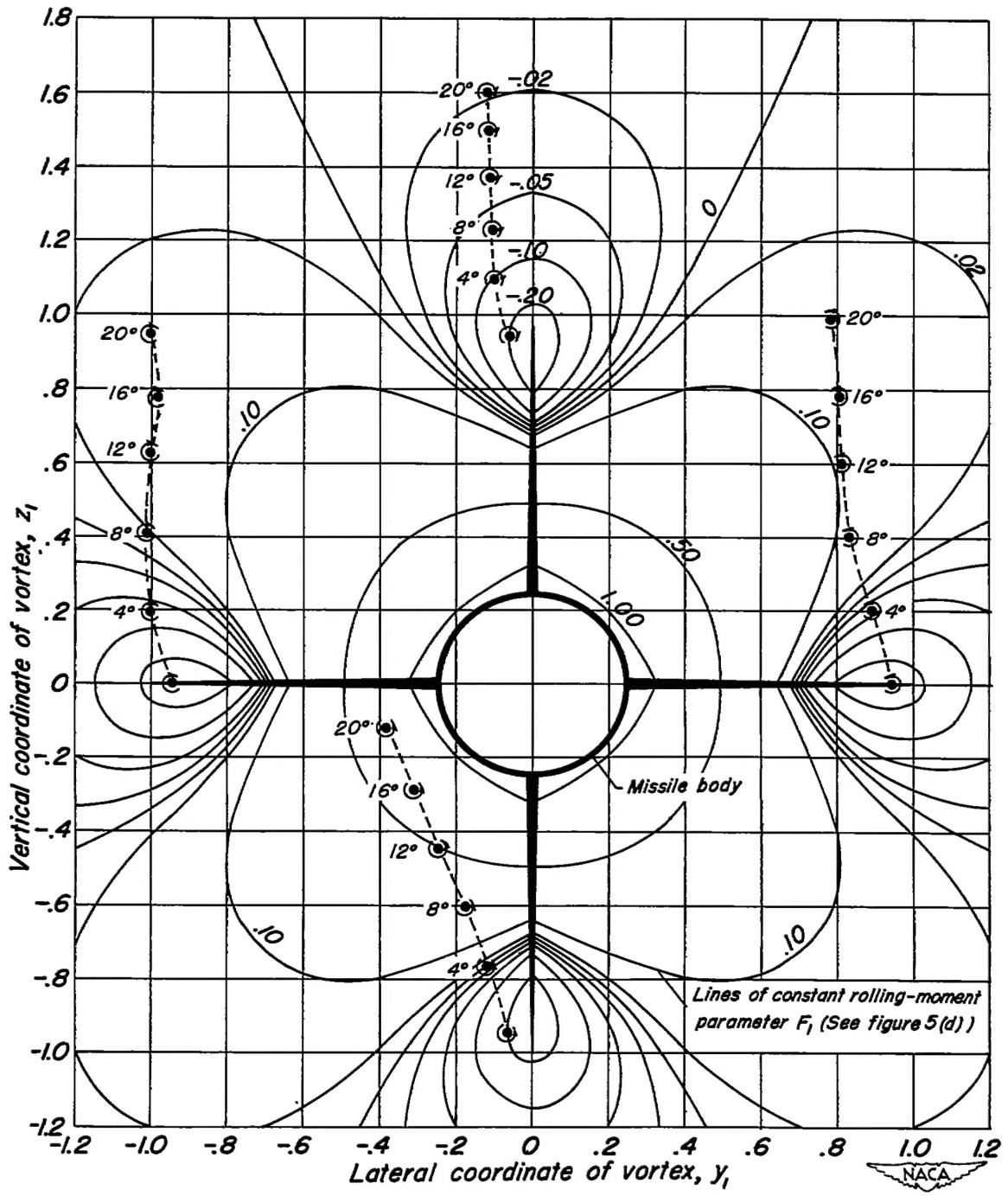

Figure 18.- Relationship between the position of the vortex cores at various angles of attack and lines of constant rolling-moment parameter, F_1, in the cross-flow plane at the center of pressure of the trailing wing of missile C at 1.4 Mach number.

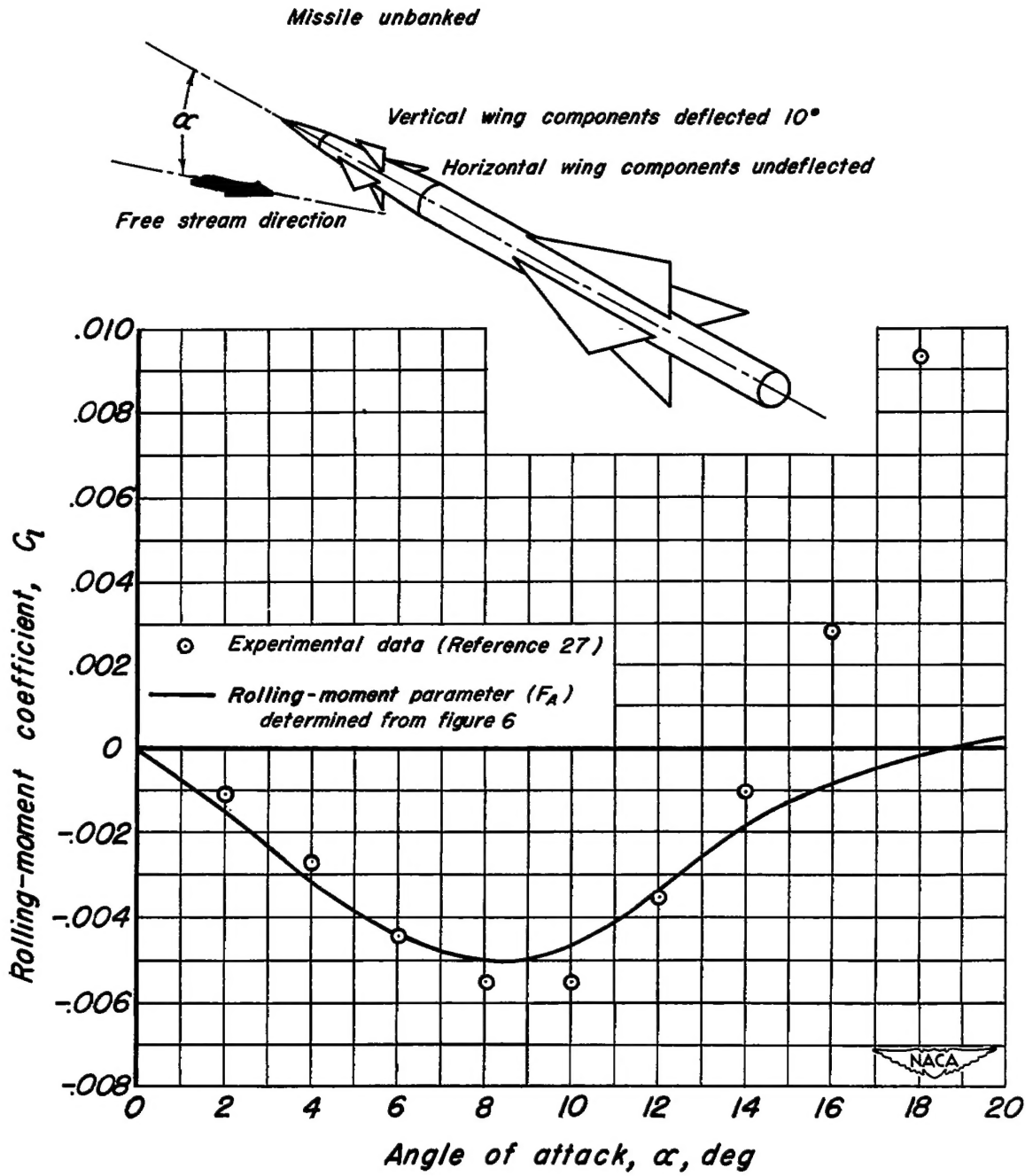

Figure 19.- Calculated and experimental tail rolling moments for missile D at 1.72 Mach number.

[redacted]

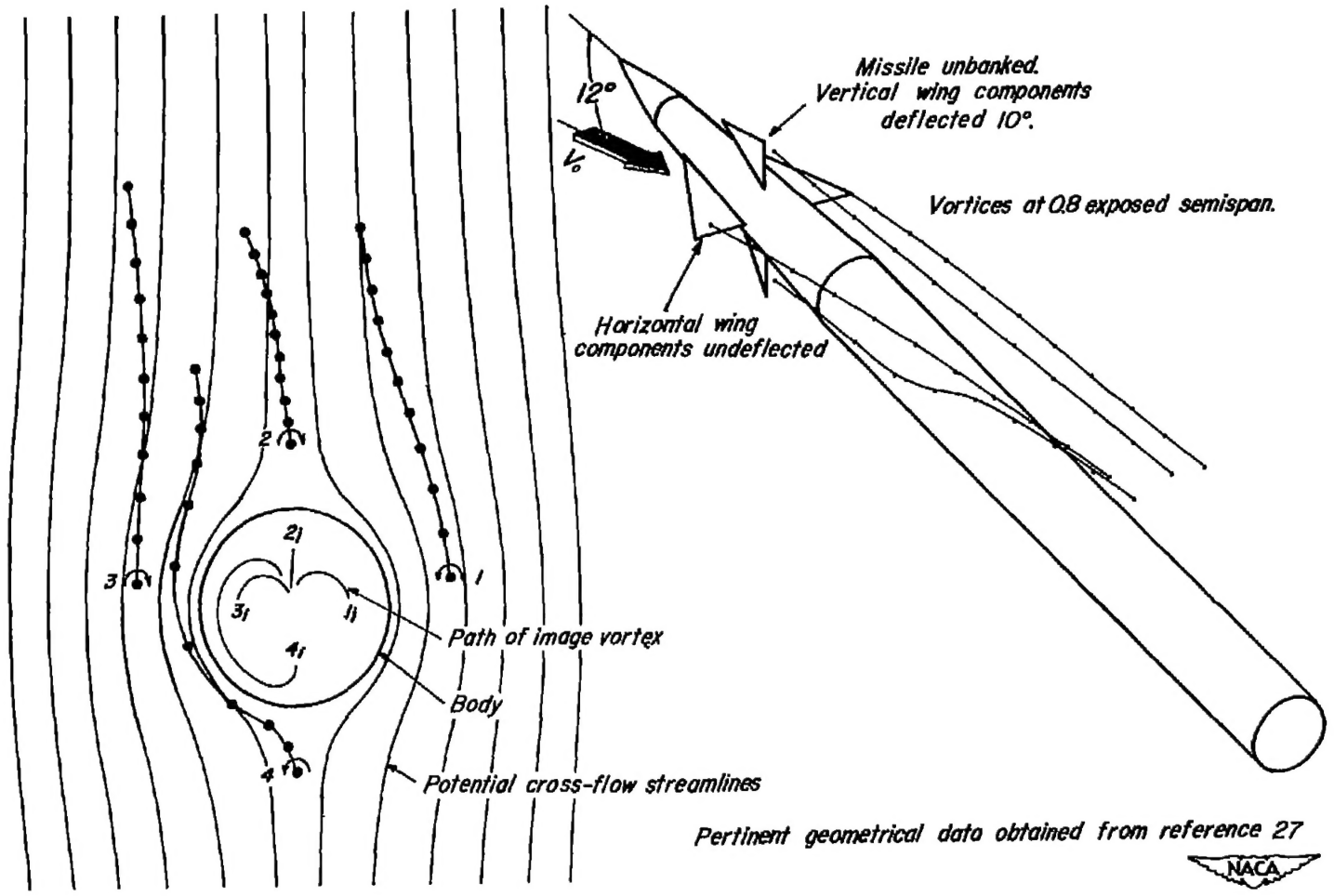

Figure 20.- Vortex paths downstream of the control fins of missile D at 12° angle of attack.

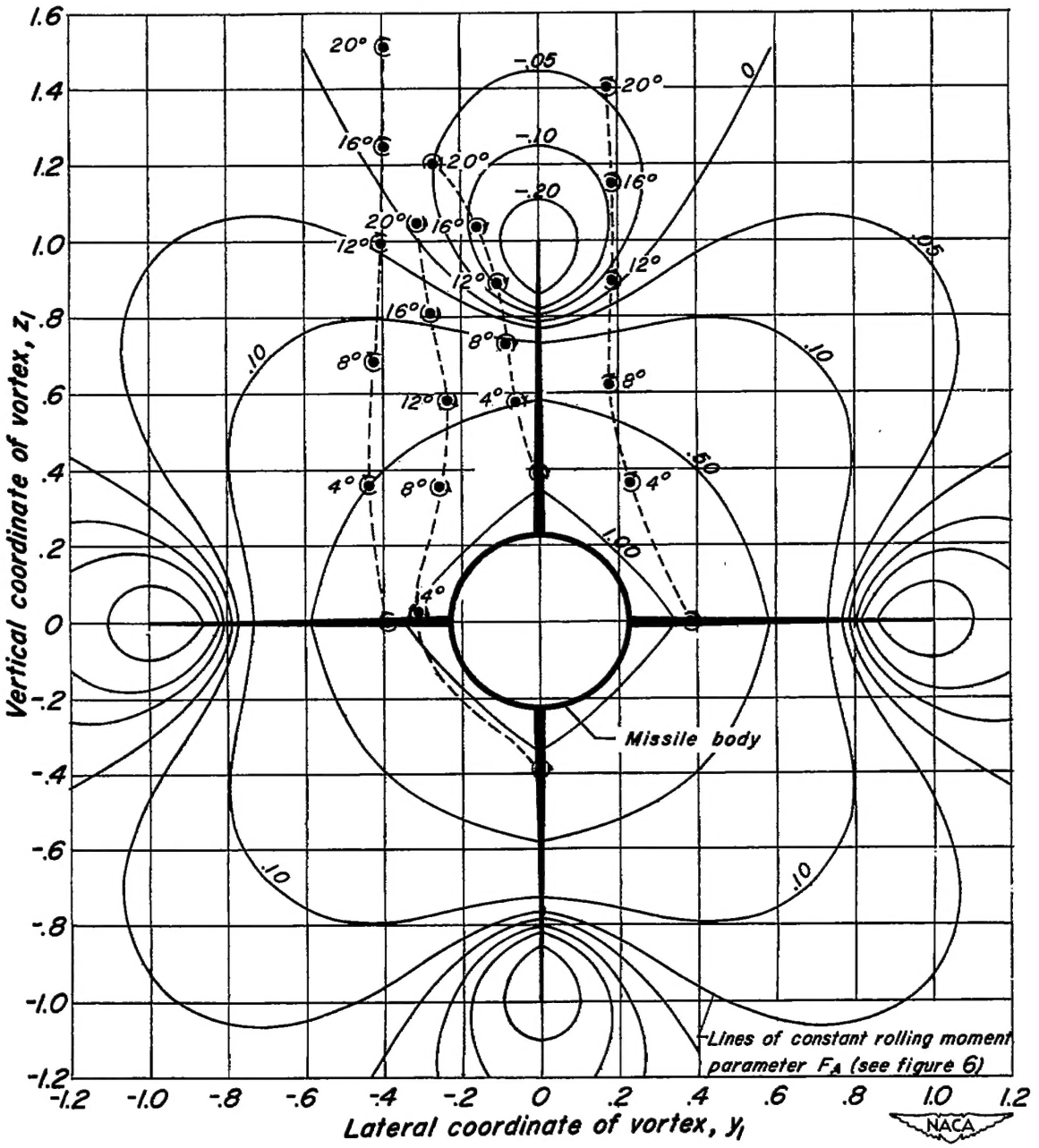

Figure 21.—Relationship between the position of the vortex cores at various angles of attack and lines of constant rolling-moment parameter, F_A, in the cross-flow plane at the center of pressure of the trailing wing of missile D at 1.72 Mach number.

NACA-Langley - 11-12-53 - 325